Challenges for Molecular Magnetic Resonance Imaging

Enzo Terreno, Daniela Delli Castelli, Alessandra Viale, and Silvio Aime*

Department of Chemistry IFM and Molecular Imaging Center, University of Torino, Torino, Italy

Received January 26, 2010

Contents

Enzo Terreno was born in Rome (Italy) in 1965. In 1991 he received a degree in Pharmaceutical Chemistry and Technology at the University of Torino (Italy), where he is currently Associate Professor of General and Inorganic Chemistry. His research interests are mainly focused on the development of paramagnetic metal complexes as probes for innovative MRI applications in the biomedical field.

Daniela Delli Castelli was born in Torino (Italy) in 1975. She received a degree in Chemistry in 2000 and a Ph.D. in 2003 from the University of Torino. She is currently a postdoctoral fellow at the Centre of Molecular Imaging of the same university. Her work is mainly focused on the development of novel nanosized MRI agents, especially based on CEST contrast.

1. Introduction

Molecular imaging aims at visualizing molecules and molecular events which occur at a cellular level.[1] To tackle this task, molecular imaging relies on the design of suitable probes which report about the physiopathological processes of interest.

When compared to other imaging modalities, the main advantage of magnetic resonance imaging (MRI) is its superb spatial resolution whereas its major drawback is represented by the limited sensitivity of its probes. Thus, chemistry is strongly challenged to find solutions able to improve the probe's response in order to enhance the role of MRI in the field of molecular imaging applications.

As the major determinants of the contrast in ^1H-MR images are the relaxation times, T_1 and T_2, of the tissutal protons, it was logical to look at paramagnetic substances as chemicals able to act as contrast agents in the regions where they distribute.

In 1979, Lauterbur showed that the presence of paramagnetic Mn(II) ions dramatically increases the proton relaxation rates in the infarcted region of a dog's heart.[2] Some years

* Corresponding author. Telephone: +39-011-6706451. Fax: +39-011-6706487. E-mail: silvio.aime@unito.it.

10.1021/cr100025t
Published on Web 04/23/2010

Alessandra Viale was born in Turin (Italy) in 1971. She received her degree in Chemistry in 1995 and her Ph.D. degree in 1998 from the University of Turin, with a thesis about organometallic chemistry. She is now a Research Technician at the University of Turin, working on the development of novel hyperpolarized probes for Magnetic Resonance Imaging applications, mainly produced by Para-Hydrogen Induced Polarization.

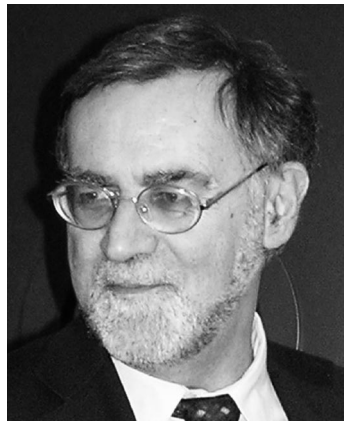

Silvio Aime is Professor of General and Inorganic Chemistry and Head of the Centre of Molecular Imaging at the University of Torino. His research interests are centered around the development of targeting and responsive MRI agents (paramagnetic complexes, CEST, hyperpolarized molecules) for *in vivo* imaging investigations (early diagnosis, monitoring of therapeutic effects, visualization of drug delivery, and cellular therapy).

later, Weinmann and co-workers reported on the effect of Gd-DTPA on MR images on humans, thus opening the way to the contrast agent that became the most used system in the clinical settings.[3] It is the prototype of the extracellular agents that distribute in blood and in the extravascular regions. It is a very stable complex (log K_f of 22) that, thanks to its high hydrophilicity, is excreted by kidneys on the time scale of a few hours. In MR images, Gd-DTPA allows us to set a good delineation of tumors as a consequence of either the high vascular permeability or the hypervascularization characterization of these lesions. As the tissue T_1 values are much longer than T_2, it was straightforward to exploit the effort of the paramagnetic contrast agents in T_1-weighted images. It was soon realized that binding a paramagnetic complex to slowly moving substrates may yield to marked relaxation enhancements of the solvent water protons on scanners operating at 0.5−1.5 T.[4] This has led us to propose a number of covalent and noncovalent adducts with synthetic or natural macromolecules, with special emphasis on the interaction with serum albumin, as the resulting supramolecular adducts are excellent reporters for angiographic investigations.

The search for more efficient agents has driven a huge number of studies aimed at getting a better understanding of the relationships between the structure and dynamics of metal complexes and the determinants of water proton relaxation rates. These results have been summarized in several reviews.[5−13] In parallel to the development of paramagnetic systems, also superparamagnetic iron oxide nanoparticles have been considered as MRI contrast agents.[14,15] Such systems act mainly as T_2* susceptibility agents, showing an excellent sensitivity in T_2*—as well as in T_2-weighted images. As particles, earlier or later, in spite of the hydrophilic cover often present on their surface, iron oxide-based contrast agents are taken up by macrophages, either circulating or tissue resident. Thus, the main diagnostic indications for iron oxide particles deal with the visualization of inflammatory states. However, their high sensitivity makes them good candidates for molecular imaging applications once the particles are bound to suitable targeting vectors.[16−20]

About a decade ago, a new class of MRI contrast agents was proposed. They no longer act on the relaxation processes but affect the intensity of the bulk water signal *via* the transfer of saturated magnetization from an exchangeable pool of protons that are properly irradiated by a radiofrequency field centered at their absorption frequency.[21] This class of agents, dubbed CEST (chemical exchange saturation transfer), represent an important innovative step because they generate a frequency-encoded contrast that makes possible the detection of more agents in the same image by selecting the proper saturation frequency of the exchanging protons.[5,22−25] Moreover, the presence of different exchanging functionalities in the same molecule allows the design of responsive systems based on ratiometric approaches that compare the relative responsiveness to a given parameter on the rate of exchange of the different kinds of mobile protons. Other agents that encode the frequency dependence are currently under intense scrutiny. The improved sensitivity of modern scanners allows the acquisition of images based on the detection of heteronuclear resonances. Attention has been initially devoted to ^{19}F-containing molecules either because this nucleus displays a sensitivity very close to the proton or because it has a quite large chemical shift range for different molecular environments.[26] However, the most innovative class of frequency-encoding agents is represented by hyperpolarized molecules containing heteronuclear resonances characterized by long T_1 values. Outstanding achievements have been obtained by using ^{13}C-labeled molecules and detecting the products of their *in vivo* transformations.[27] These results opened the way to characterize the metabolic state at the cellular level, an approach of tremendous potential if the clinical translation will be successful.

This survey aims at outlining the most innovative approaches that have been undertaken in the recent history of MRI contrast agents. For any class of agents, selected examples will be reported, with no intention to be exhaustive, but with the aim of showing how chemistry can tackle the challenges of sensitivity and specificity required by the new generation of MRI contrast agents. The role of MRI in the armory of diagnostic modalities for the medicine of the forthcoming years largely depends on how chemistry will provide advanced tools to meet the medical needs.

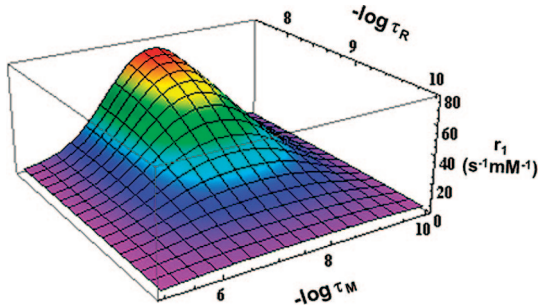

Figure 1. 3D simulation illustrating the effect of the rotational mobility (τ_R) and the residence lifetime of the water molecule coordinated to a metal ion (τ_M) for a generic Gd(III) complex.

2. Challenges in the Field of Paramagnetic T_1 Agents

Paramagnetic complexes of metal ions with symmetric electronic ground states, such as Gd(III) and Mn(II), have been successfully used as MRI contrast agents since the late 1980s in virtue of their outstanding ability to shorten the longitudinal relaxation time T_1 of water protons dipolarly interacting with the unpaired electrons of the metal ion.

As far as their use in molecular imaging is concerned, the main issue is represented by the high sensitivity required when the biological targets are present at very low concentrations. Therefore, a major challenge with this class of agents for the forthcoming years continues to be the achievement of the highest attainable sensitivity.

The efficiency of these metal chelates to catalyze the ^{1}H water relaxation process is commonly expressed in terms of the longitudinal relaxivity (r_1) that reports about the enhancement of the water proton relaxation rate (T_1^{-1}) in solutions containing 1 mM of the paramagnetic solute.

In the last two decades and more, the task that attracted most of the efforts from chemists working in this field has been to design metal complexes endowed with high r_1 values. To this purpose, it is worthy to recall that the relaxation enhancement induced by a paramagnetic center can be accounted for in terms of the Solomon−Bloembergen−Morgan theory.[28] According to that, the observed r_1 values are the result of a rather complex interplay of several structural and dynamic parameters of the metal complex, among which the more relevant ones are the number of labile water molecules coordinated to the metal (q), their residence lifetime at the metal site (τ_M), the tumbling motion of the complex (τ_R), and the relaxation characteristics of the unpaired electrons of the metal ion (T_{iE}, $i = 1, 2$). Theoretical considerations have guided the route for the optimization of the determinants of the relaxation processes in order to improve the sensitivity of T_1 agents. The theory foresees the attainment of r_1 values of about 100 s^{-1} mM^{-1} at magnetic fields around 1 T (for a single inner sphere water molecule) once the dynamic parameters (τ_M, τ_R, and T_{iE}) have been optimized (Figure 1). However, despite the large efforts to design metal complexes with optimized properties, this target has only been approached in very few cases.[29,30]

2.1. Optimizing the Rotational Mobility

For applications at 0.5−1.5 T, one of the key tasks for achieving high relaxivity is represented by the control of the effective tumbling motion of the metal−water proton vector of the system. Usually, the lengthening of the rotational motion is pursued through a covalent or noncovalent binding of the metal complex to macro-/supramolecular carriers, but in most of the cases, the rotational mobility of the paramagnetic agent is higher than that of the carrier molecule due to the flexibility of the linking spacer that enables the complex/carrier binding.[31−34] In addition, the metal−water proton vector itself may rotate independently and faster than the whole complex,[35] thus limiting the advantage to bind the complex to the macromolecular carrier. Several strategies can be adopted in order to overcome this problem. Spherically shaped carriers such as globular proteins or dendrimers may ensure an isotropic and slow tumbling motion, especially if the metal complex is rigidly bound to the carrier. For instance, the relaxivity (per metal ion) of a Gd-DOTA-like complex bound via an amido linkage to a linear dextran polymer was reported to be *ca.* 40% lower (10.6 vs 16.5 s^{-1} mM^{-1}) than that of the same agent bound to a "spherical" dendrimer, despite the latter carrier having a much smaller molecular weight (15 vs 52 kDa).[36,37] A useful way to limit the rotational freedom of a chelate bound to a macromolecular carrier was suggested by Caravan and co-workers, who demonstrated that an increase in the rigidity of the complex, and consequently in its relaxivity, can be obtained by exploiting a multisite binding.[38] This approach requires the synthesis of ligands endowed with two or more binding moieties tailored for the selected carrier (e.g., proteins, polycyclodextrins, etc.). In addition to the relaxivity enhancement, such agents display an improved binding affinity toward the carrier, thus increasing the overall efficiency of the system.[39]

The optimization of the matching between the mass of the complex and its rotational mobility has been pursued through the design of systems where the metal−water proton vector lies at the molecular barycenter. Examples of this approach are represented by some compounds developed by Guerbet (P760, P775, and P792)[40,41] and the dendritic Gd(III) complexes reported by Fulton et al.[42] Despite the relatively low mass of these systems (3−7 kDa), very high relaxivity values (20−40 s^{-1} mM^{-1}) were obtained. It is worth noting that, in addition to the optimal rotational coupling between the metal center and the ligand, the relaxivity of such systems improved thanks to the contribution arising from labile protons interacting via hydrogen bond with the large number of hydroxyl groups on the surface of the ligands (Chart 1). Another approach to optimize the rotational motion of the paramagnetic center was proposed by Jacques and Desreux, who prepared a bis-chelate for Gd(III) ion in which the two coordination cages were linked by a bis-pyridyl moiety.[43] In the presence of Fe(II) ions, three ligands wrap around the transition metal, thus forming a rigid structure containing six Gd(III) ions. This concept was later extended by Merbach and co-workers using a $q = 2$ Gd(III) chelate.[44,45] These multitopic complexes share two important advantages for their potential clinical use: (i) high relaxivity values at clinical fields and (ii) high relaxivity values per mass unit of agent. The first benefit is related to the observation that, at magnetic field strengths higher than 2 T, the Solomon−Bloembergen−Morgan theory predicts an inverse correlation between r_1 and τ_R (Figure 2).[46] This means that the optimization of a paramagnetic contrast agent for applications at 3 T requires rotational tumbling around 1 ns, whereas slower motions are necessary for achieving high relaxivity values at lower fields. The second advantage is correlated to the observation that in MR molecular imaging experiments a high number of paramagnetic centers needs to be delivered at the biological

Chart 1

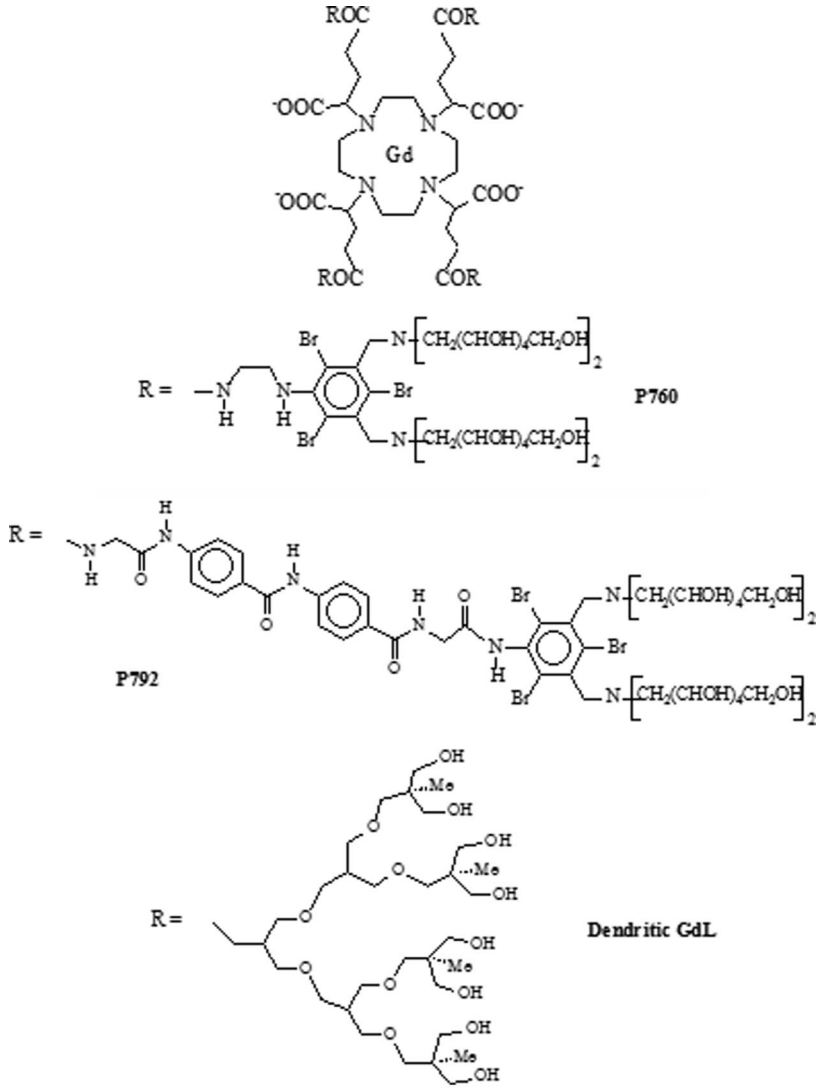

target. This means that the performance of medium-size agents with densely packed metal centers may be a better solution than the use of large macromolecules with a low "density" of paramagnetic ions. This guess led to the definition of "relaxivity density", i.e. the relaxivity of the agent normalized to its unit mass rather than to the millimolar concentration of the metal center.[47] Thus, Gd(III) complexes of multitopic low molecular weight chelates able to bind more Gd ions display high relaxivity density and may represent an interesting indication for future work.

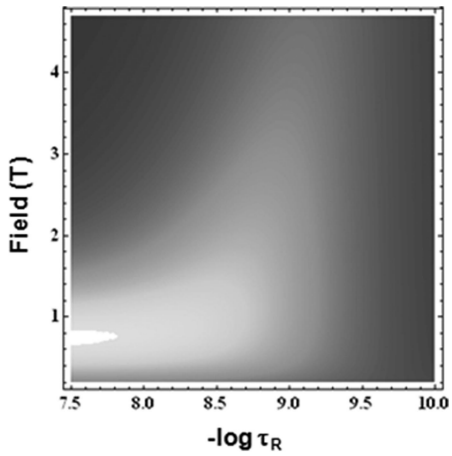

Figure 2. 2D relaxivity surface map illustrating the correlation between magnetic field strength and rotational mobility. With increasing field, the relaxivity peak broadens and its maximum moves to faster reorientational motions.

2.2. Effect of τ_M on the Attainable Relaxivity

Another parameter that needs to be optimized for attaining high relaxivities is the residence lifetime, τ_M, of the water protons at the metal site. Thanks to the understanding of the relationships between τ_M and the structure of the complex, it is now possible to design octadentate chelates with optimized residence lifetime for the coordinated water molecule.[48−53] However, when the complexes are interacting with macromolecules, τ_M values can be severely affected, usually elongated, as a consequence of the formation of the supramolecular adduct. Typical examples are reported for Gd(III) complexes noncovalently bound to human serum albumin (HSA).[49,54−56] The reduced lability of the water molecule at the metal site could be related to the formation of hydrogen bonds or charge transfer effects with polar groups of the protein at the binding region. These effects have been observed for several complexes bearing noncoordinating polar moieties.[56,57] In addition, to modulate the

Chart 2

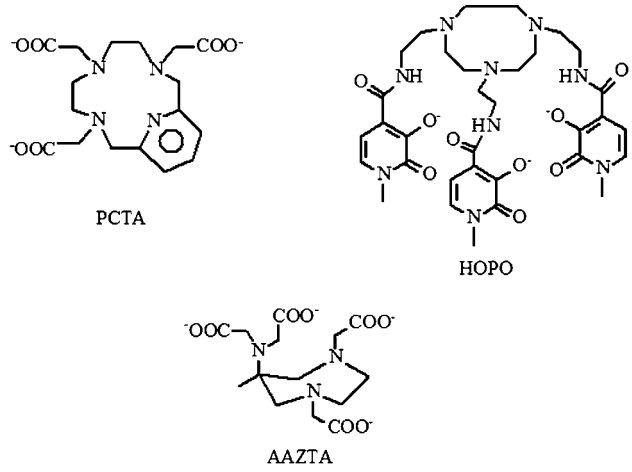

molecular reorientational time and the residence lifetime of water at the metal site, the interaction with a macromolecular carrier may affect other determinants of the relaxation process. For instance, it has been reported that donor groups of the protein located in the proximity of the binding site of the complex can replace water molecules coordinated to the metal center. This process, which has been observed for some Gd(III) complexes with $q > 1$, "quenches" the expected relaxivity enhancement brought about by the restricted rotational motion of the complex, owing to an overall reduction of the inner sphere hydration.[58,59] On the other hand, the macromolecule may own labile protons in the close proximity of the binding site of the complex, thus providing additional contributions (usually described as second sphere contributions) to the overall relaxivity. The magnitude of these effects can be evaluated by using related metal complexes (based on Gd(III) or Mn(II)) without water molecules in the inner coordination sphere of the metal.[60−62]

2.3. Increasing Relaxivity through the Increase of the Hydration of the Paramagnetic Metal Ion

In recent years, there has been an active search for coordination cages able to form highly stable Gd(III) complexes endowed with an increased hydration sphere. The prototypes of these ligands are based on the macrocyclic heptadentate PCTA[63−66] and AAZTA[67−69] ligands and on the hexadentate HOPO-based ligands (Chart 2).[70−73] As far as this last family, highly remarkable is the work carried out by K. Raymond and co-workers, who, through an in-depth understanding of the structural determinants of the coordination bonding scheme, have been able to design optimized systems including a derivative with $q = 3$ characterized by a remarkable r_1 value (at 20 MHz) of 13.1 s^{-1} mM^{-1}.[74]

The success of these highly hydrated Gd(III) complexes relies on the concomitant high relaxivity, high stability against transmetalation, and no tendency to form ternary adducts with anionic substrates. These advantages have prompted their use as a basic scaffold for the synthesis of highly efficient agents using the typical approaches for optimizing the rotational mobility.[62,75−78]

2.4. Nanosized Systems

The challenge of high relaxivity has also been tackled by using the huge armory of tools offered by nanotechnology. Many nanoscaffolds have been considered so far in order to optimize the relaxivity and to modulate the pharmacokinetic properties of the imaging reporter, including dendrimers,[79] proteins,[62] micelles,[80] nanovesicles,[81] nanoemulsions,[26] carbon-based nanosystems,[82] and metal-based nanoparticles.[83]

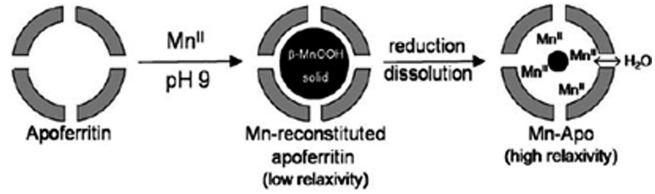

Figure 3. Schematic view for the preparation of Mn(II)-loaded apoferritin. Reprinted with permission from ref 88. Copyright 2009 Wiley & Sons.

In this very wide scenario, two examples deserve attention for both the surprisingly high performance and for their interesting biological implications. The first case deals with the use of the naturally occurring apoferritin as carrier for Gd(III) agents. It has been shown that the relaxivity of the low molecular weight complex Gd-HPDO3A (approved for the clinical use as ProHance) entrapped inside the apoferritin cavity is 20-fold enhanced (*ca.* 80 s^{-1} mM^{-1}).[84] The reason for such a great enhancement is not yet clearly understood, but interestingly, an outstanding relaxivity was also observed upon entrapment of a $q = 0$ complex in the apoferritin cavity.[85] This finding was taken as an indication that a dominant contribution to the observed relaxivity does not rely only on the exchange of the inner sphere water molecule. It has been hypothesized that the relaxation efficiency is amplified by the dipolar contacts between the metal center and the high number of mobile protons of amino acid residues facing the inner apoferritin cavity.[86] Thanks to its high biocompatibility, this probe is currently under intense scrutiny in MR molecular imaging applications.[87]

Unfortunately, any attempt to increase the relaxivity per particle failed, as the used preparation method does not allow the inclusion of more than 8−10 Gd-HPDO3A molecules per apoferritin cavity. The task of internalizing a much higher number of paramagnetic centers inside the apoferritin cavity has then been pursued by dissolving the solid β-MnOOH phase that one may create by exposing the protein to a concentrated solution of Mn(II) salts at basic pH values. The reduction/dissolution processes operated by suitable reducing agents lead to hundreds of Mn^{2+} ions entrapped inside the apoferritin cavity (Figure 3). Although each Mn^{2+} ion displays a r_1 value lower than that observed for Gd(III) complexes in the same apoferritin environment, the relaxivity per protein molecule can be increased by an order of magnitude.[88]

Very high relaxivities (*ca.* 160−170 s^{-1} mM^{-1} at clinical fields) were also reported for single wall carbon nanotubes (SWNTs) doped with Gd(III).[89] Again, the operating relaxation mechanism is not fully understood. The loaded Gd(III) ions might form small clusters in the proximity of side-wall defects, and such clusters could display a superparamagnetic behavior. Interestingly, it has been reported that the hydrophobic environment of the carbon nanotubes channel is responsible for fast rates in the diffusion of water and protons inside the tubes, and this finding might also play a role in accounting for the high relaxivity of such systems. Unlike the case of apoferritin, there is concern about the *in vivo* biocompatibility and the overall stability (especially against aggregation phenomena) of SWNTs that could limit the great potential shown *in vitro*.

Anyway, the examples reported in this section suggest that other routes to high relaxivities may be pursued for paramagnetic systems in addition to the optimization of the parameters of the relaxation process on the basis of the Solomon−Bloembergen−Morgan approach. More work is certainly necessary to get a good understanding of the underlying relaxation pathways, but these achievements already have the merit of supporting the view that classes of contrast agents endowed with much higher relaxivities may be available in the near future.

2.5. Mn^{2+}-Complexes: An Alternative to Gd-Based Agents?

Though most of the work involving T_1 agents has been carried out with Gd(III)-based agents, the use of Mn(II) probes has recently attracted new interest. Likely, the recent FDA warning on the increased risk of nephrogenic systemic fibrosis (NSF) and nephrogenic fibrosing dermopathy (NFD) for patients with renal failure and subjected to contrast enhanced MRI exams prompted the search for alternatives to Gd(III).[90] Mn(II) ion owns 5 unpaired electrons with long electronic relaxation times, and it is used as such in functional MR imaging (the so-called manganese enhanced MRI) in animal studies.[91] From the chemical point of view, the typical coordination number of Mn(II) is 6, and therefore, it is quite challenging to design highly stable complexes with one or more water molecules coordinated to the metal. Actually, the only Mn(II) complex approved for clinical use, MnDPDP (Teslascan), is an outer sphere complex ($q = 0$, low relaxivity) that can be considered as a sort of proagent. In fact, the main clinical application of this agent is in the detection of liver lesions because the agent is readily internalized by healthy hepatocytes where it is rapidly metabolized and transmetalated by zinc.[92] The released Mn(II) ions can readily interact with intracellular species (likely proteins) that are responsible for the large T_1 enhancement detected in healthy liver. Therefore, the lesions (e.g., tumor metastasis) are visualized as hypointense spots.

Nanotechnology has opened new interesting possibilities also for Mn(II)-based systems. Some examples of "hard" Mn(II) nanoparticles designed for molecular imaging experiments have been recently published.[93−95] Conversely, examples of soft materials are those represented by self-assembled paramagnetic monomers. In this context, Pan and colleagues have recently reported paramagnetic nanoparticles consisting of nanocolloids made of Mn(II) oxide or Mn(II) oleate coated with phospholipids.[96] These systems showed interesting relaxometric properties with particulate relaxivities of *ca.* 450 000 s^{-1} mM^{-1} for the more efficient Mn-oleate nanocolloid. The good sensitivity displayed by these systems was demonstrated through the *in vitro* visualization of human thrombi by using biotinylated nanoparticles able to recognize (*via* avidin) a biotinylated antifibrin antibody.

Thus, Mn^{2+}-based agents, in spite of the slightly less stronger relaxation enhancement properties with respect to the case of Gd^{3+}-based ones, are recovering interest because Mn^{2+} is an essential metal ion and nature has developed suitable pathways to maintain its homeostasis. Although it will be hard to find ligands able to bind Mn^{2+} ions with a strength higher than that shown by naturally occurring endogenous substrates, it seems likely that applications of systems releasing Mn ions will be further developed. The LD_{50} for $MnCl_2$ is low (0.22 mmol/kg), but one may design low toxicity approaches based on the confinement of Mn^{2+} ions inside proper nanocarriers whose release may be operated by endogenous or external stimulii only when the systems have reached the biological target.

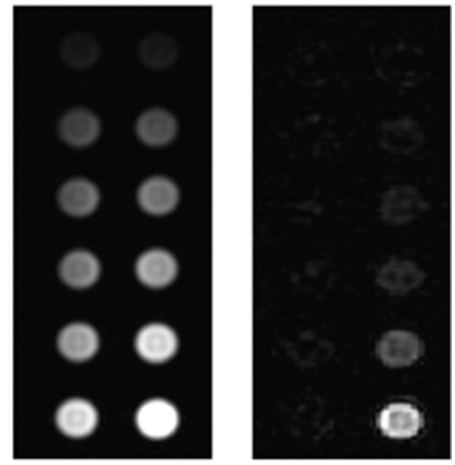

Figure 4. *In vitro* MR images of a phantom consisting of solutions containing increased concentrations (from 0 to 160 mM downward) of the Gd(III) complex Vasovist alone (left column) or in the presence of rabbit serum albumin 4.5% w/v (right column). Left: Conventional T_{1w} image. Right: Field-dependent image where only samples containing the protein are detected. Adapted with permission from ref 98. Copyright 2009 Wiley & Sons.

2.6. Field-Dependence of Relaxivity

The task of improving the sensitivity of T_1 agents has also been addressed by matching at best the magnetic field dependence of the relaxation parameters. MR molecular imaging protocols rely on amplification procedures that require the accumulation of the agent at the biological target. Ideally, the probe should be silent in the background and MR visible in the presence of the specific target (off → on state). Practically, this is difficult to achieve and one has often to deal with images in which the MR agents contribute to enhance the background signal in areas different from the target region. A means of improving the probe specificity in MR molecular imaging has been recently proposed by Alford et al., who used an auxiliary electromagnet to slightly modify the strength of the static field in a standard MRI scanner.[97] In the presence of a Gd(III) complex whose relaxivity is field dependent only when it is bound to the biological target, the detection of the activated (bound) contrast agents is significantly improved. As proof of concept, Figure 4 shows the results obtained on a phantom containing different concentrations of the Gd(III) complex Vasovist in the presence of rabbit serum albumin. The strong noncovalent interaction with the protein makes the relaxivity of the complex field dependent, thus facilitating the MR visualization of the target.

The dramatic increase of sensitivity that can be achieved by measuring the slope of the relaxivity curve rather than its absolute value points out the advantages that may arise from the development of field-cycling MRI scanners. This task is currently pursued by D. Lurie and co-workers at the University of Aberdeen (U.K.).[98] It is expected that the availability of field-cycling MRI scanners, that will allow the full exploitation of the NMRD profiles of paramagnetic substances, will address new directions to yield contrast agents characterized by peculiar frequency dependence and able to quantitatively report on the interaction with target molecules in the region of interest.

In summary, a lot of work carried out in the last two decades has shown that Gd^{3+} and Mn^{2+} complexes immobilized on slowly tumbling macromolecules display a relaxivity peak centered at 20−40 MHz. At higher fields, the relaxivity of these systems rapidly decreases, and this behavior could be considered a drawback for clinical MRI scanners operating at 3 T. The situation is even worse with animal scanners that usually operate at 4.7 or 7 T or even higher fields. This behavior of Gd/Mn-based agents strongly limits their applications in the field of molecular imaging, as the major applications are represented by targeting experiments in which the paramagnetic probe is suitably designed to recognize macromolecular epitopes at the cellular level. In the forthcoming years it might become possible to exploit the peculiar relaxation enhancement of slowly moving paramagnetic complexes through the introduction of scanners operating at 1 T. This possibility will open new horizons as concern the development of molecular imaging applications in the longitudinal studies of small animal models. One may expect that this approach may become highly competitive with other *in vivo* imaging approaches to follow the up/down regulation of receptors/transporters that define the staging of important diseases, including tumors, thanks to the implicit quantitation of Gd centers at the site of interest that can be made in a MR image.

2.7. Responsive Agents

Another important challenge for T_1 paramagnetic agents deals with the design of responsive probes, i.e. systems whose relaxivity reports about a specific parameter of the microenvironment in which they distribute. Despite the large number of publications demonstrating the great potential of Gd(III) complexes to report about changes of diagnostically relevant physicochemical variables *in vitro*, only very few studies have been reported so far *in vivo*.

One of the first example of an *in vivo* application of a responsive Gd(III) complex was reported by Meade and co-workers,[99,100] who synthesized paramagnetic agents (α- and β-EGadMe) bearing a galactopyranosyl moiety and able to generate a contrast enhancement in the presence of the enzyme β-galactosidase, commonly used in cellular biology for reporting gene expression. The relaxivity increase in the presence of the enzyme was the result of an increase in the overall hydration state of the metal center following the cleavage of the sugar moiety. The α-complex was injected in *X. laevis* embryos with and without the mRNA expressing the enzyme, and the embryos injected with mRNA showed a remarkable T_1 enhancement.[100]

Another relevant contribution to the field of enzyme-activatable agents has been provided by Weissleder et al., who demonstrated, both *in vitro* and in animal models of different diseases, the high potential of paramagnetic Gd(III) complexes to report about the activity of the mieloperoxydase enzyme, a key-marker of inflammation processes and involved in numerous pathologies.[101,104]

In a first step, the activation mechanism of the complexes involves the formation of a radical species that can proceed differently depending on the considered complex. Two mechanisms were identified for explaining the relaxation enhancement: one related to the oligomerization of the complex and another related to the formation of cross-linked structures with proteins. Interestingly, the complexes exhibit peculiar mixings of such mechanisms. As the two activation modes lead to a differential clearance of the agent from the tissue, such agents could be used for clinical applications that require different time windows.

Chart 3

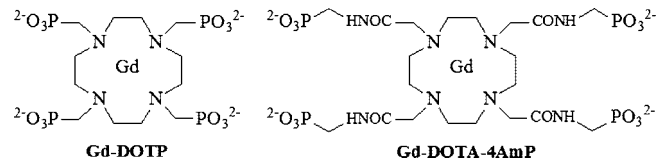

The most challenging issue related to this application remains the need for measuring the MR contrast that reports about the variable of interest only, i.e. without any contribution arising from a difference in the local concentration of the responsive agent. This task has been tackled by using different approaches. The first one was proposed by Gillies, Sherry, and co-workers, who obtained a pH map of mouse kidneys and a rat glioma through the consecutive injection of two Gd(III) complexes, a pH responsive and a nonresponsive one, respectively (Chart 3). Under the assumption that the two complexes have the same biodistribution, the contrast difference generated by the nonresponsive agent is used for taking into account changes in the local concentration. The knowledge of the concentration, voxel by voxel, allows access to a relaxivity-based image that directly reports about the local pH differences.[105,106] Though the obtained results were quite interesting, this approach has some flaws. The responsive and the nonresponsive probe have different structures, and the assumption that their biodistribution is the same could not be strictly valid. Furthermore, the injection of two different contrast agents in the case of probes with an intermediate−slow body clearance may require a large time interval between the two administrations. During this time, physiopathological changes may occur and the basic assumption of identical biodistribution of the two agents may be jeopardized.

Another approach deals with the possibility of acquiring a concentration independent ratiometric MR response based on the determination of the T_1/T_2 ratio after the injection of a single agent.[107,108] The rationale of this approach relies on the possibility to make dependent on a specific variable (e.g., pH or temperature) only one of the two relaxation times. In this way, the ratio will get rid of the local concentration effects of the agent (provided that concentration changes occur slowly enough with respect to the time required for obtaining the parametric T_1 and T_2 maps), but the dependence on the variable of interest is maintained. Particularly suitable systems for this approach are nanosized systems whose structure can be designed to be responsive through T_1 (e.g., following a pH dependence of its overall mobility), whereas the T_2 is mainly determined by other parameter(s).

A third approach is based on the design of responsive dual $^{19}F/^{1}H$ probes that provide information on the absolute probe concentration in a given region of interest through the acquisition of the ^{19}F images.[109] Hence, if the ^{19}F-label is properly combined with a responsive Gd(III) agent in the same molecule or in the same supramolecular construct, the variable to be measured can be determined by the detection of ^{1}H and ^{19}F images. A proof of concept of this method to assess pH has been recently reported (Figure 5).[110] It is based on the use of a poly-β-cyclodextrin support loaded with a Gd(III)-based pH responsive agent and a ^{19}F-containing molecule. As shown in Figure 6, a good assessment of the pH in the capillaries of the phantom has been obtained. Likely, the loading of an amphiphilic responsive probe to

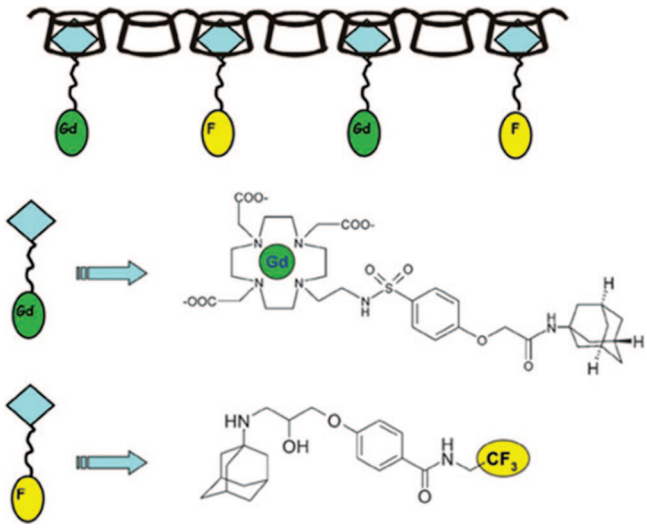

Figure 5. Schematic representation of the strategy adopted for developing a dual $^{19}F/^{1}H$ concentration independent pH responsive MR probe. Reprinted with permission from ref 110. Copyright 2009 Royal Chemical Society.

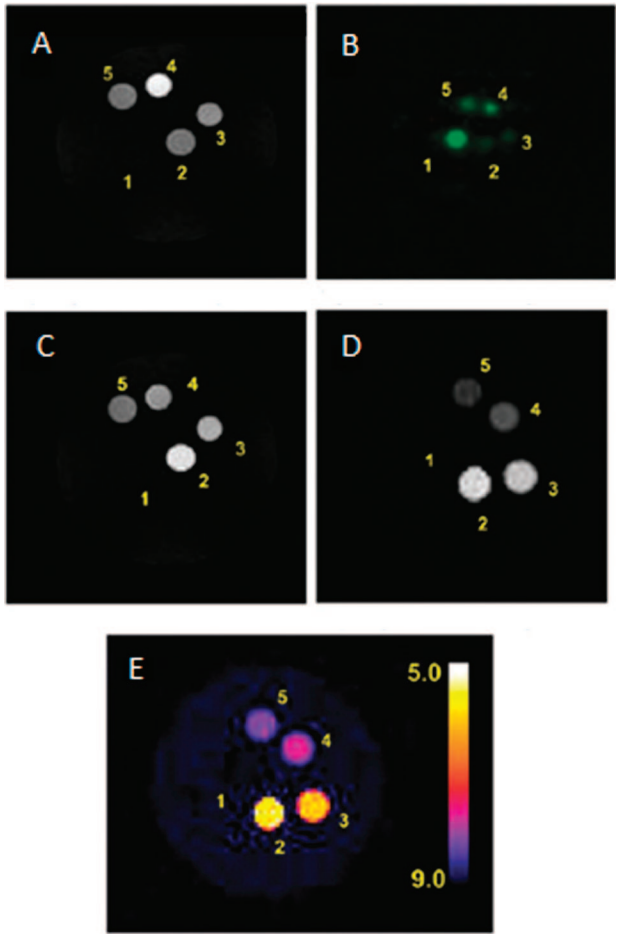

Figure 6. MR images of a series of glass capillaries containing the following solutions: (1) PF_6^- 25 mM, (2) poly-CD 10 mM + ^{19}F reporter 2.5 mM + Gd-complex 0.5 mM, pH 6.8, (3) poly-CD 13 mM + ^{19}F reporter 3.25 mM + Gd-complex 0.65 mM, pH 7.2, (4) poly-CD 40 mM + ^{19}F reporter 7.5 mM + Gd-complex 1.5 mM, pH 7.6, (5) poly-CD 20 mM + ^{19}F reporter 5 mM + Gd-complex 1 mM, pH 8.2. (A) T_{1w} proton MR image at 7 T, (B) ^{19}F MR image at 7 T, (C) T_{1w} proton image A normalized according to the signal from image B, (D) T_{1w} proton image at 1 T, (E) pH map derived from image D. Reprinted with permission from ref 110. Copyright 2009 Royal Chemical Society.

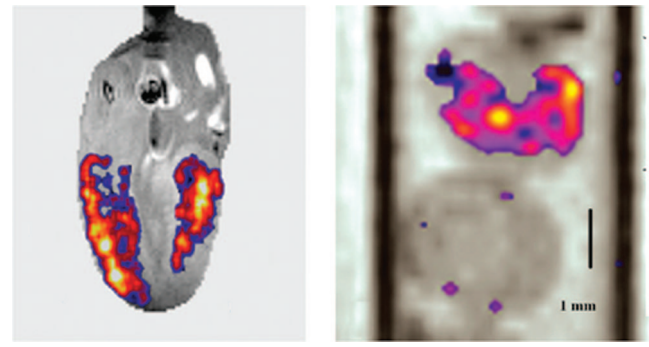

Figure 7. Left: MR image of an arrested rat heart perfused with a 100 μM solution of GdDOTA-4AmP. The color map shows the regions that became acidic after 15 min of ischemia. Right: MR image of alginate beads empty (lower beads) or encapsulating rat pancreatic islets (upper beads) both perfused with a 50 μM solution of GdDOTA-4AmP. The colored map identifies voxels where the signal map increased above noise after the glucose concentration in the perfusate was increased from 5 to 25 mM. More acidic regions correspond to yellow; less acidic to purple. Adapted with permission from ref 111. Copyright 2009 American Chemical Society.

^{19}F-based nanoparticles would represent a good extension of this class of agents.

Sometimes it may not be necessary to measure an absolute value of the tissue variable in order to obtain diagnostically useful information. For example, if the scope is the visualization of regions with altered pH values, it could be sufficient to target a single pH responsive agent (whose contrast is activated at low pH values) in order to visualize the areas characterized by abnormally low pH values. This method has been tested *ex vivo* upon exposing two different perfused tissues, rat heart and pancreatic islets, to a pH sensitive Gd(III) complex (GdDOTA-4AmP; see Chart 3) and collecting their T_1-weighted images.[111] Control hearts perfused with 100 μM agent did not show regions characterized by different contrast enhancement, while ischemic hearts clearly showed brighter regions that are ascribable to areas with low pH values (Figure 7, left). Similarly, rat pancreatic islets embedded in alginate beads and perfused with 50 μM agent showed a detectable T_1 enhancement only after exposure to high concentrations of glucose (Figure 7, right). It is known that the glucose-mediated insulin secretion is accompanied by the release of protons (as well as Zn^{2+} ions) from insulin granules, and the consequent local increase in proton concentration can then be visualized. An improvement of the methodology has been attained through the synthesis of a system in which a bifunctional derivative of GdDOTA-4AmP has been covalently linked to a macromolecular carrier (G5-PAMAM dendrimer) to exploit the benefit of a restricted rotational motion. The resulting macromolecular agent retained the pH sensitivity of the parent complex, but the responsiveness (Δr_1 between pH 6 and 7.4) was increased by *ca.* 50%.[112] As a consequence, much less agent (0.1−0.3 μM of dendrimer) is necessary for detecting the pH variations shown in Figure 7.

In summary, it appears likely that more work has to be done in this field to develop new responsive agents able to get rid of the concentration issue and pursue the transformation of the observed relaxation rates into relaxivity values. It is straightforward to outline the importance of introducing into the clinical practice images that map the changes of physicochemical parameters such as pH, temperature, or variation in the activity of a specific enzyme.

3. Challenges for T_2 Agents

Whereas the paramagnetic metal complexes described in the previous section aim at yielding hyperintensity (bright contrast) in T_1-weighted MR images as a consequence of a low R_2/R_1 value, it was early suggested that hypointense (dark) contrast could have been obtained with contrast agents able to yield high R_2/R_1 or R_2^*/R_1 ratios. Such T_2/T_2^* agents, which affect contrast in T_2/T_2^* weighted MR images, can be addressed in a number of ways. For instance, the R_2 of water protons increases in the presence of prototropic exchange, and simple molecules containing many exchangeable protons may induce, at high magnetic fields, significant shortening of T_2.[113] Much stronger T_2-effects may be obtained by using paramagnetic metal complexes with an appropriate exchange rate of the inner sphere water.[114] Both approaches recall suggestions, reported decades ago, to address the suppression of the water signal in ^{1}H NMR spectra. The selective shortening of the transverse relaxation time of the water ^{1}H resonance allows its cancellation in the spectra of biological fluids by applying a properly designed excitation pulse sequence (water attenuation by T_2 relaxation, WATR).[115] Another approach to increase the R_2/R_1 ratio was tackled by means of $H_2{}^{17}O$. In this case, T_2 is shortened by the modulation of $^1H-^{17}O$ scalar coupling by the prototropic exchange.[116] This method is very efficient, but it has not been further developed, probably due to the high costs of water labeled with ^{17}O.

Very efficient routes to enhance R_2/R_2^* values are provided by the paramagnetic particulates that will be discussed in the next sections.

3.1. Iron Oxide Nanoparticles

Superparamagnetic iron oxide nanoparticles (SPIO) have been often utilized as MR imaging probes for molecular imaging experiments. These particles are able to efficiently shorten T_2, and particularly T_2^*, of water protons.[15] The contrast generation mechanism is related to the magnetic properties of the particles that induce a strong magnetic susceptibility effect on the water protons that diffuse around the particle. The relaxometric and the pharmacological characteristics of SPIOs are mainly controlled by their size. SPIOs typically consist of a crystal core of magnetite (Fe_3O_4) and γ-maghemite (Fe_2O_3) coated with a suitable material with an overall diameter between 60 and approximately 250 nm. Smaller particles (20−50 nm) are defined as ultrasmall SPIO (USPIO) and are characterized by a lower r_2/r_1 ratio. In addition, also micrometer-sized particles (MPIO) have been demonstrated to be useful in the fields of cellular labeling[117,118] and intravascular targeting.[119] The relevant role played by the particle size introduces the first challenge for this class of agents, i.e. the possibility of controlling dimension, dispersion, and the overall reproducibility of the preparation step. In fact, the synthesis of SPIO of a defined size is often a process difficult to control mainly for the colloidal nature of ferrite. Thus, the search for experimental conditions leading to a monodisperse population of crystal cores of suitable and controlled size is still an important task. Another relevant aspect is the design of optimized processes for improving the crystallinity degree of the ferrite core that is proportional to the overall magnetization of the particle and, therefore, to the efficiency of the probe. Finally, a critical point deals with the selection of a reproducible procedure that should be industrialized without any complex purification procedure. At present, several procedures have been used to produce magnetic nanoparticles from solutions, aerosol, or vapor phase.[120]

Once the preparation of the crystal core is optimized to be usable for *in vivo* applications, the particle needs to be coated with a suitable biocompatible material. The coating is fundamental to prevent particle aggregation and sedimentation and to provide a stable suspension ready for clinical use. To this purpose, several materials have been used and different interaction forces exploited, including hydrogen bonds, electrostatic forces, and pseudocovalent linkages. Furthermore, the surface coating is very important for defining the pharmacokinetic behavior of the particle, even though all SPIOs show a remarkable tropism toward the monocyte phagocytic system (MPS) and macrophage-rich organs. For instance, the introduction of PEG chains reduces the ability of serum protein to recognize the particle, thus prolonging the blood lifetime to an extent that depends on the PEG conformation (mushroom- or brushes-type) and density on the particle surface.[121]

Besides PEG, other typical coating polymeric materials that have been used so far include dextran and hydrophilic derivatives, starch, arabinogalactan, glycosaminoglycan, organic siloxane, and sulphonated styrene-divinylbenzene.[122] In addition, also monomers such as amino acids, α-hydroxy-acids, hydroxamate, dimercaptosuccinic acid, and citric acid have been successfully utilized for coating SPIOs.[123−126]

The research in the field of SPIOs is missing a robust structure−pharmacokinetic correlation. To achieve this task, it will be necessary to improve the currently available tools (or develop new ones) for describing accurately the basic physicochemical properties of the particles (surface composition, charge, hydrophilic/hydrophobic balance, etc.).

One of the most important drawbacks in using SPIOs is inherently related to the contrast mechanism that they generate. In fact, their effect in MRI images consists of a signal loss, and this prevents their clinical use in low signal body regions, in organs with intrinsic high magnetic susceptibility (e.g., lung), or in the presence of hemorrhagic events and partial volume effects. To overcome these limitations, specific off-resonance pulse sequences able to generate a positive (bright) contrast in the presence of SPIOs have been proposed.[127] Interestingly, this approach has been demonstrated to yield a greater contrast-to-noise ratio than the standard gradient echo sequence commonly used for detecting negative contrast.[128] More recently, another approach, called inversion recovery ON-resonant water suppression (IRON)-MRI, has been developed to obtain a positive contrast in the presence of superparamagnetic particles.[129] This method has been successfully applied in rabbit to identify macrophage rich atherosclerotic plaques with high accuracy upon administration of MION-47 (monocrystalline iron oxide nanoparticles). No significant signal enhancement was measured in remote areas without plaques by histology and in controls without atherosclerosis.[130]

Another possibility to detect a bright contrast has been demonstrated by Senpan, Caruthers, et al., who prepared novel iron-based nanoparticles in which the metallic core, suitably coated with oleate, was further embedded in a hydrophobic matrix composed of vegetal oil and partially cross-linked phospholipids.[131] Surprisingly, the encapsulation of the iron oxide crystals diminished the T_2 relaxation more than T_1, thus allowing the probe visualization in T_{1w} images. This finding has a remarkable role for facilitating the imaging

of intravascular targets, because the T_1 effect of the background (e.g., blood) is much less persistent (*ca.* 1 h) than the T_2* contrast detected after the iv injections of SPIO particles, whose blood lifetime may be until 24 h.

Besides their clinical use, that is primarily focused on the detection of liver and lymph node lesions, SPIOs are the golden standard probes for cellular imaging experiments.[132] Despite the great success of SPIOs in this field, several issues still need to be tackled. For instance, though SPIOs are well tolerated and do not affect significantly cell functions, it has been reported that they may increase the formation of free hydroxyl radicals and reactive oxygen species, thus increasing the rate of apoptosis and inducing alterations in cellular metabolism.[133] Moreover, dissolved Fe^{2+} ions from the particle degradation may have potential toxic effects on the cells. It has been demonstrated that the labeled cells can be protected from the potential toxicity of SPIOs through an inert gold coating.[134] In addition, the gold-coated shell enhances MRI contrast significantly. More importantly, gold has well-defined surface chemistry toward thiol or amine moieties. This offers an attractive and convenient route for pursuing further functionalization of the SPIOs with biomolecules through thiol- or amine-coupling chemistry.[135]

Targeted imaging with iron oxide particles is often pursued because the particles may have a sensitivity in the nanomolar range. Recently, it has been shown that cardiomyocite apoptosis in heart failure (in mice) can be imaged by means of annexinV-labeled nanoparticles (cross-linked iron oxides, CLIO).[136] Important achievements have been reported by Weissleder and co-workers in the use of magnetic nanoparticles in cellular and molecular imaging of atherosclerotic plaque and myocardial injury.[137]

Iron oxide nanoparticles encapsulated in liposomes, the so-called magnetoliposomes, offer very interesting and peculiar opportunities in the medical field. In addition to their ability to generate T_2/T_2* MR contrast,[138] such systems have been shown to have favorable properties for acting as "theranostic" agents, as they can locally generate heat in response to an externally applied oscillating magnetic field (hyperthermia),[139] and they can be accumulated in specific body regions through the guide of an external magnetic field (magnetic targeting).[140] Both these properties, also in combination, have a great potential for combating cancer.[141]

However, one of the current issues in using magnetoliposomes as combined imaging/therapeutic systems deals with the high amount of iron oxide required to create local hyperthermic effects. The involved strong magnetic field gradients may create large distortions in the MR images.

Their good sensitivity and the ability to be efficiently taken up by cells, either by passive or active uptake,[142] are at the basis of their success in cellular labeling experiments. As nanoparticles, SPIOs are very efficiently taken up by phagocytic cells such as macrophages, whereas specific targeted approaches need to be adopted for other cells (e.g., stem cells, neurons, pancreatic β-cells, ...) for which there is a large interest in following their *in vivo* fate after implantation. An issue related to the use of SPIOs as cellular labels deals with the fact that particles, eventually released from the labeled cells that die after the inoculation, may be taken up by macrophages, thus potentially leading to wrong interpretations of the cell-tracking experiment. However, a recent study has demonstrated that only less than 10% of iron oxide particles can be found in activated macrophages after inoculation of SPIO-labeled stem cells.[143]

In addition to nanoparticles whose metal core is fully based on iron oxides, other nanosystems with a different chemical composition of the magnetic core have been developed and tested.[144] For instance, it has been reported that, due to the higher magnetization, iron nanoparticles have higher T_2 relaxivity than analogous systems containing iron oxides.[145] Furthermore, such systems efficiently induce local hyperthermic effects. Alloy-based nanomaterials are good candidates for developing T_2 contrast agents with higher relaxivity. Several bimetallic ferrite nanoparticles, including $CoFe_2O_4$, $MnFe_2O_4$, and $NiFe_2O_4$, have been investigated as potential T_2 contrast agents, and some of them, especially $MnFe_2O_4$ nanoparticles (MnMEIO), have been found to display a very high magnetization and large T_2 relaxivity values.[146,147] However, it is worth pointing out that such systems could be very useful for preclinical experiments, whereas their clinical translation will require a careful assessment of their acute and long-term toxicity.

3.2. T_2 Agents: Alternatives to Iron Oxide Nanoparticles

Though SPIOs represent by far the most used T_2/T_2* agents, other systems sharing the same (or similar) T_2-relaxation mechanism have been recently proposed. Among them, paramagnetic liposomes appear to have a good potential for being considered for further *in vivo* investigations. In these nanosystems, the local magnetic field gradients able to dephase the water protons diffusing around the vesicles are generated by the high amount of paramagnetic complexes encapsulated in the liposomes. The T_2 efficiency of these agents is dependent on many variables, including the vesicle size, the concentration of the entrapped agent in the inner core of the vesicle, its paramagnetism (expressed by the μ_{eff} value of the paramagnetic center), and the external static magnetic field strength (Figure 8). Thanks to the high effective magnetic moment, Dy(III) containing complexes are the most efficient agents to be encapsulated. The T_2 relaxation enhancement efficacy at 7 T of a typical unilamellar liposome loaded with Dy-HPDO3A and normalized to a 1 mM solution of liposomes ranges from 10^7 to 10^9 s^{-1},[148] which are values quite comparable, if not even larger, to those reported for SPIOs.

Dy(III)-loaded liposomes share with iron oxide particles large r_2/r_1 ratios and a similar biodistribution (rapid accumulation in liver and spleen). Unlikely for SPIOs, the liposomal agents may have some advantages, especially in the field of "theranostic" agents, including (i) the easiness to coload the vesicle with a drug, (ii) the possibility to make the T_2 contrast dependent on responsiveness to the vesicle integrity (potential use for imaging the drug release), (iii) good biocompatibility because liposomes are intrinsically well tolerated and the paramagnetic content can be selected among the clinically approved and safe Gd(III) agents (going from Gd(III) to Dy(III) is not expected to affect the toxicity of the complex).

Presently, though very few reports on T_2 paramagnetic liposomes are available in the literature, the potential of these systems for cell targeting experiments has been demonstrated on tumor cultured cells.[148] Most of the challenges related to the *in vivo* use of liposomes (vesicle stability, stealthiness toward macrophages, targeting, etc.) still have to be tackled.

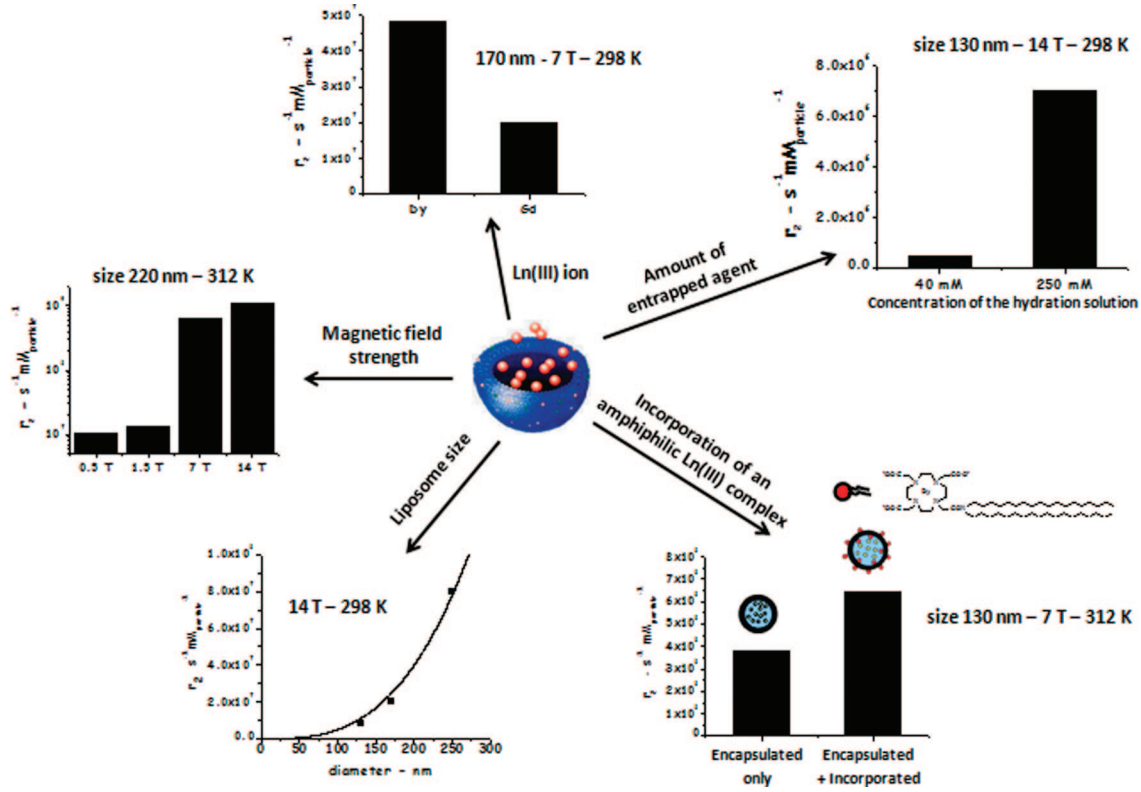

Figure 8. Paramagnetic liposomes as T_2 agents. The figure illustrates the effect of the variables that influence the T_2 efficiency for such nanoprobes.

3.3. Magnetic Particle Imaging

Recently, a new imaging modality called magnetic particle imaging (MPI) has been proposed.[149] It relies on the nonlinear magnetization of ferromagnetic nanoparticles and provides the direct visualization of the distribution of the particles in the given anatomical region. It has been shown that, upon injection of iron oxide particles in the blood, the particles appear as a bright signal in the image, from which their local concentration can be calculated. It is expected that the MPI approach will allow the assessment of coronary blood flow, myocardial perfusion, ejection fraction, and targeted probes with great sensitivity and accuracy. The basic scanner setup requires a static magnetic field, an oscillating field, and signal receiving coils. The detection modality closely resembles susceptometry-based methods, thus leading to the direct mapping of iron particles whereas in conventional MRI the contrast is generated through the indirect effect on tissue water molecules.

4. Challenges for CEST Agents

Chemical exchange saturation transfer (CEST) agents represent an emerging class of MRI contrast media. The basic properties and main application fields of these probes have been thoroughly described in several reviews recently appearing in the literature,[22,23,150] and also in this special issue of *Chemical Reviews*, this topic has been exhaustively treated.[151]

Briefly, the CEST contrast arises from a selective saturation (through the application of a suitable radiofrequency field) of a proton pool in slow-to-intermediate exchange (in the NMR frequency time scale) with the bulk water. The saturated magnetization of the irradiated spins is then transferred to the water resonance, thus decreasing its intensity. By such a mechanism, the contrast is encoded with the resonance frequency of the exchangeable spins of the agent, and this peculiarity introduces important advantages toward conventional proton relaxation enhancement agents such as (i) the possibility of yielding a MR response without requiring a precontrast scan and (ii) the possibility of detecting more than a single agent in the same region of interest.

The first point is expected to have a great impact in order to speed up the clinical exams and improve the patient compliance. The second item can significantly expand the diagnostic potential of the technique, allowing the setup of a wide array of experiments that would benefit from the simultaneous visualization of different agents (e.g., targeting of multiple epitopes for improving the tumor characterization, use of differently sized agents for dynamic investigations, etc.).

In this section we focus our attention on the challenges that have to be tackled in order to translate to the clinics the great potential of such probes.

The currently still open issues related to the *in vivo* translation of the favorable properties of CEST agents can be classified into three groups depending on their origin: (i) instrumental/technical, (ii) chemical, and (iii) biological.

4.1. Technical Issues

The group of instrumental technical issues refers to problems related to pulse sequences and, more in general, to the experimental setup required for an optimized detection of CEST contrast.

In any sequence designed for CEST experiments, the "core" is represented by the saturation scheme through which the specific frequency corresponding to the resonance of the exchanging proton pool is saturated. Generally, this part of the sequence is placed just before a conventional MRI pulse

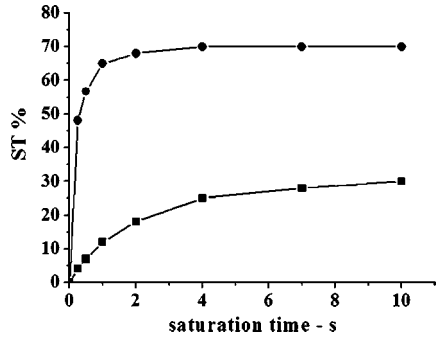

Figure 9. Dependence of the CEST effect (expressed as ST%) on the saturation time for two different CEST agents: a PARACEST complex (Yb-DOTAMGly, circles) and a DIACEST molecule (iopamidol, squares). Experimental conditions: field strength 7 T, $T = 312$ K, [CEST agent] = 30 mM, B_2 amplitude 25 μT.

sequence, possibly a fast one such as turbo spin−echo, ultrafast gradient-echo, or echo planar imaging (EPI). An interesting perspective to improve the temporal resolution of the overall sequence is the design of an interleaved sequence in which the saturation is spread out during the whole imaging acquisition, as has been recently proposed.[152] Whatever is the selected pulse sequence, one of the crucial key points that could be a limit for the successful *in vivo* use of a CEST procedure is represented by the specific absorption rate (SAR) constraints.

The SAR level induced by a pulse sequence on a given specimen is the sum of the power deposited by each pulse of the sequence, and it is dependent on many factors, including the pulse duration, the pulse type (e.g., rectangular or shaped), and the total scanning time.[153] It is noteworthy that, besides the specific pulse sequence, SAR values are related to the field strength as well as the sample characteristics.

However, the maximum power deposited in a CEST experiment is directly dependent upon the saturation time and the pulse(s) amplitude used within the saturation scheme. Concerning the saturation time, it is noteworthy that the saturation transfer builds up with an hyperbolic temporal evolution, whose ramp rate is related to the exchange rate of the irradiated mobile protons and the longitudinal relaxation rate of the bulk water protons. On this basis, diamagnetic CEST agents (the so-called DIACEST) often display a slow exchange rate and low R_1 value. This means that the maximum CEST contrast is reached after longer saturation times than those for paramagnetic CEST (PARACEST) probes (Figure 9). On the other hand, the advantage of PARACEST systems to reach a good saturation transfer in short times is counterbalanced by the need for using large pulse amplitudes, which, in turn, lead to a detrimental SAR increase. Usually, this observation is related to the fast exchange of the already broad paramagnetically shifted mobile protons. For this reason, the exchange rate of such protons needs to be optimized in order not to overcome SAR limits.

A representative example has been reported by Li et al., who demonstrated that, through a proper chemical design, the exchange rate of a set of paramagnetically shifted CEST-active protons can be optimized in order to improve the detection of the CEST contrast lowering the SAR values.[154]

Though the SAR value is dependent on many variables, pulse amplitudes below 24 μT have been demonstrated to be safe in animal models.[155] However, it has to be noted that the SAR value for a given pulse sequence is dependent on the duty cycle of the magnet, and therefore, lower SAR values can be attained by lengthening the repetition time TR, with a worsening of the temporal resolution of the overall experiment.

Another way to reduce the amount of deposed energy is to use shaped pulses instead of rectangular ones. Shaped pulses can also better fit the shape of the resonance to be saturated. Usually, this approach works better when the shape of the CEST-active pool is very broad, as observed for many PARACEST agents.[156]

Since a good saturation efficiency requires the use of short shaped pulses (generally milliseconds scale), the saturation transfer is then accomplished by using a train of shaped pulses interleaved by a very short (few microseconds) delay.

Another technical challenge very relevant in this field, unlikely to conventional contrast mechanisms, is represented by the homogeneity of the static B_0 field, usually related to the characteristics of the imaging coil or caused by a shimming/susceptibility mismatch. In fact, a poorly homogeneous field introduces spatially related differences in the chemical shift of the bulk water resonance that represents in CEST experiments the reference frequency at which the saturation offsets are calculated. In order to take into account such effects and avoid the contrast artifacts they generate, different approaches have been proposed. They are primarily based on the pixel-by-pixel quantification, and successive correction, of the B_0 inhomogeneity using specific MRI methods,[157] by preceding the CEST experiment with a fast Z-spectrum for determining the exact frequency resonance of the bulk water[158] or by using the same CEST experiment for carrying out a postprocessing correction.[159]

Besides the B_0 homogeneity, also the sample shimming plays a key role in the correct quantification/detection of the CEST contrast. In fact, a nonoptimal shimming could affect the shape of the resonance of the bulk water, thus leading to a frequency-dependent asymmetry that may be the source of contrast artifacts.

Usually, the artifacts associated with B_0 and shimming inaccuracies are more relevant for the detection of CEST contrast of agents with a small frequency offset (e.g., DIACEST, spherical lipoCEST, or endogenous agents) even though this observation is partly balanced by the fact that such systems do require low amplitude (and less perturbing) saturation pulses.

Among the technical aspects, it is also important to mention the role of B_1 field homogeneity, particularly relevant in consideration of the constant increase of the magnetic field strength in clinical MRI, and that one of radiation dumping effects.[160]

Finally, it is worth noting that novel CEST-like approaches have been recently proposed. One example has been reported by Vinogradov et al., who demonstrated the possibility to create a MR contrast in the presence of a PARACEST agent through the application of a low power pulse train positioned at the resonance frequency of the bulk water.[161]

This method (named OPARACHEE, from On resonance PARAmagnetic CHemical Exchange Effects) was successively implemented for *in vivo* applications,[162] yielding good results in the images of mice kidneys after iv injection of a relatively low concentration (2 mM) of a T_m-based complex.[163]

A further elaboration of the CEST experiment has led to a novel approach, called pCEST (positive CEST).[164] The method is based on the detection of the so-called apparent T_1, i.e. the longitudinal relaxation time measured by applying

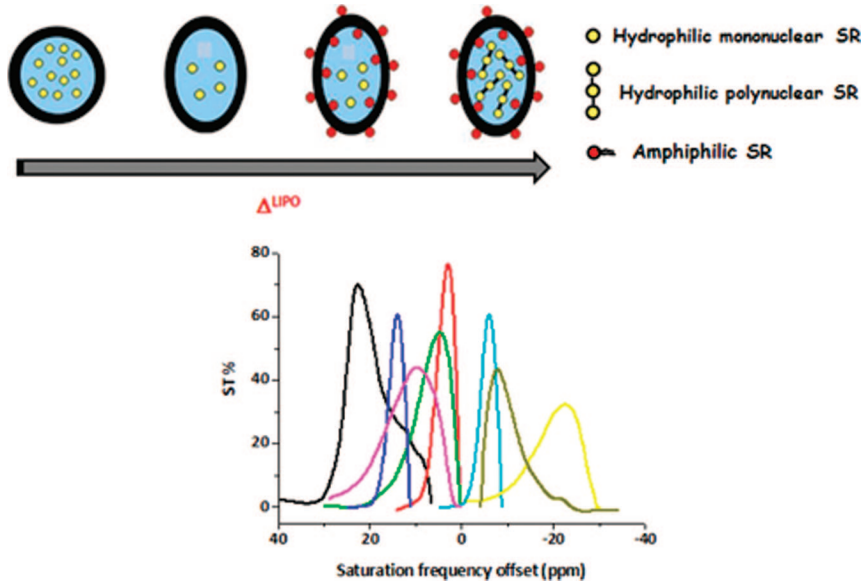

Figure 10. Schematic view of the achievements carried out for increasing the range of the chemical shifts for the water molecules in the intraliposomal compartment for LipoCEST agents.

a radiofrequency irradiation during the inversion pulse of the imaging sequence. The apparent T_1 is usually shorter than the corresponding value measured without the RF irradiation, and it is further shortened when the RF pulse is set at the resonance frequency of the exchangeable protons of the CEST agent. Through a proper setting of the experiment, it is possible to get a positive "apparent T_{1w}" contrast in the presence of the CEST agent.

4.2. Chemical Issues

The "chemical" challenges are mainly related to the design of CEST agents able to generate a very efficient CEST contrast without requiring large amplitude saturation pulses (and possibly allowing a multiple detection) as well as to optimize the structural properties in order to address the *in vivo* biodistribution and accumulation of the probe at given diseased regions.

The sensitivity issue for the CEST agents was early recognized already in the seminal work of Ward et al.,[21] and it has driven most of the research performed so far in this field. In close analogy to what has been done with T_1 MR agents, macro-/nanomolecular systems containing a large number of CEST active mobile protons (including paramagnetically shifted ones) have been designed and tested to improve the attainable sensitivity. In general, the sensitivity per single saturated proton is in the millimolar range,[4] and this means that sensitivities in the micromolar concentrations are expected, and experimentally observed, for systems (both dia- and paramagnetic) containing thousands of magnetically equivalent or pseudoequivalent exchangeable protons, such as polyaminoacids,[165,166] nucleic acid-like systems,[167] dendrimers,[155,168] polymers,[169] adenovirus particles,[170] and nanoemulsions.[171] A breakthrough in this field was achieved by combining the NMR shifting abilities of paramagnetic chelates with the peculiar properties of liposomes. The resulting lipoCEST agents represent the most sensitive class of CEST agents developed so far, with a subnanomolar contrast detection limit for the most efficient systems.[172] The reason for such efficient saturation transfer relies upon the possibility to saturate the whole pool of the exchangeable intraliposomal water protons, whose number (per vesicle) is ranging from 10^7 to 10^9 depending on the liposome size.[173,174] The required $\Delta\omega > k_{ex}$ condition is met by encapsulating a paramagnetic shift reagent that, unlike conventional PARACEST agents, does not necessarily possess mobile protons, as its role is that of inducing a paramagnetic shift of the intraliposomal water protons. In addition, the coalescence condition is avoided by the relatively low water diffusivity through the liposome bilayer that can be advantageously and properly modulated by modifying its chemical composition.[175]

Since their discovery in 2005, the basic properties and the potential applications of LipoCEST agents have been carefully investigated, giving special emphasis to the possibility of modulating the chemical shift of the water resonance in the intraliposomal compartment. It has been found that a significant extension of the chemical shift values of such protons can be obtained either by encapsulating neutral polynuclear paramagnetic shift reagents[176] that increase the payload of an intraliposomal shift reagent or by exploiting the bulk magnetic susceptibility (BMS) contribution to the chemical shift.[177] This latter approach involves the preparation of nonspherical vesicles in which the extent of the induced shift is dependent on the vesicle shape and their preferential orientation within the magnetic static field. Nonspherical liposomes were prepared using osmotic shrinkage, and their orientation in the field, which is dependent on the magnetic susceptibility anisotropy of the liposome membrane,[178] was modulated by changing the magnetic properties of amphiphilic lanthanide-based complexes suitably incorporated in the vesicle.[179,180] By using this approach, a range of chemical shifts of about 70 ppm has been attained, thus facilitating the multiple visualization of lipoCEST agents in the same region (Figure 10).[181]

One of the current challenges in using lipoCEST agents is represented by the intrinsically low stability of these vesicles that are quite prone to be taken up and degraded, especially by macrophage-rich organs (the liver and spleen). However, the loss of the ability to act as a CEST agent can also be exploited in order to make their MRI response sensitive to the release of the liposomal content (e.g., a drug). An illustrative example of the potential of lipoCEST in the field of imaging of drug delivery has been recently published (Figure 11).[182]

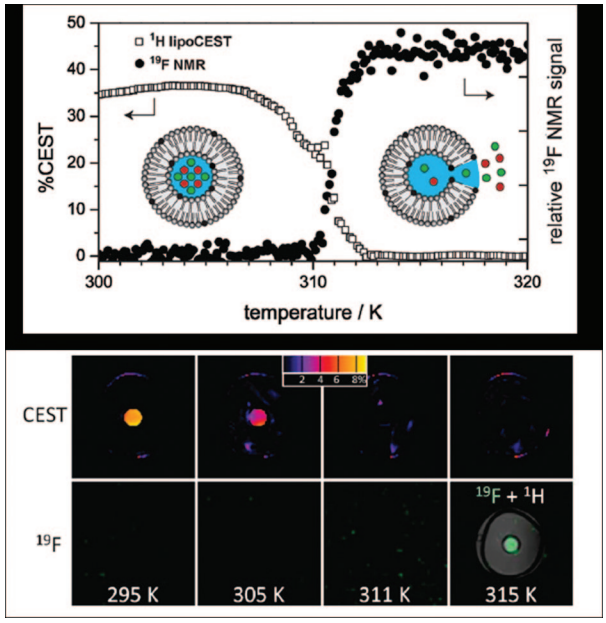

Figure 11. Top: Temperature dependence of the CEST effect and ^{19}F signal intensity for a thermosensitive LipoCEST agent encapsulating NH_4PF_6. Bottom: proton CEST map (overlay with standard proton image) and ^{19}F MR images on a clinical 3 T scanner at different temperatures. Adapted with permission from ref 182. Copyright 2009 American Chemical Society.

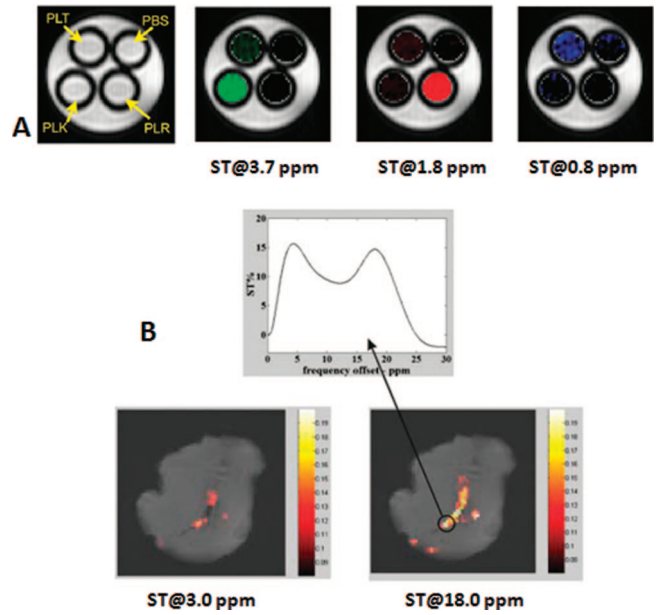

Figure 12. Examples of multiple detection of CEST agents. (A) MR-CEST images of a phantom containing three peptides (2.5 mg/mL) bearing mobile protons resonating at different frequencies (amide protons at 3.7 ppm, guanidine protons at 1.8 ppm, and hydroxyl protons at 0.8 ppm). Adapted from ref 184. (B) MR CEST maps overlaid on a standard MR image of a bovine muscle injected with a solution containing two LipoCEST agents with different resonance frequencies of their intraliposomal water protons (3 ppm, spherical liposomes, and 18 ppm, osmotically shrunken liposomes). Adapted with permission from ref 181. Copyright 2008 Wiley & Sons.

Apart from this example, there is still a large interest in developing nanovesicular CEST agents with an improved biological stability, and potential solutions could be found using polymerized liposomes or a novel class of polymersomes.[183]

As far as it concerns the design of CEST agents for multiplex detection, a number of interesting examples can be found in the literature using either diamagnetic[184] or paramagnetic[108,181,185,186] agents (Figure 12). In this area, in addition to the optimization of the NMR properties of the probes, there is the expectation that technical improvements devoted to the optimization of the temporal resolution and saturation selectivity of the CEST experiment will be fundamental for the future clinic success of these protocols.

4.3. Biological Issues

This last challenge deals with the drawbacks associated with the characteristics of the biological environment, and it mainly deals with the saturation transfer contribution arising from the exchangeable protons of the tissue background. This effect, better known as magnetization transfer contrast (MTC), is already routinely exploited in several clinical protocols, especially in MR angiography and for multiple sclerosis diagnosis.[187]

MTC and CEST contrast are somehow related: in the former modality, the endogenous solidlike (and consequently very broad) resonance of the exchangeable protons immobilized on tissues is excited by using a low-amplitude pulse centered tens of kilohertz off-resonance from the bulk water. The resulting water signal intensity is then compared with the one arising from the experiment carried out without saturation, and the obtained contrast is usually interpreted in terms of the "mobility" of the water protons. This acquisition protocol is particularly useful to improve the blood-to-tissue contrast. Conversely, in a typical CEST experiment, the contrast arises from comparing two experiments in which the saturation pulse is always "on" but centered at two frequency offsets equally spaced from the "bulk" water resonance, at high and low field, respectively. One of the two offsets corresponds to the resonance of the CEST agent. Hence, the presence of the MT contrast can interfere with an accurate detection of CEST contrast as long as the shape of the resonance of the MTC protons pool is no longer symmetric and it is not centered, as appears to be the case,[188] at the same resonance frequency of the bulk water. Several approaches may be followed to overcome this problem. Again, the use of low amplitude saturation pulses has a dramatic role in reducing the MT contribution (Figure 13), and furthermore, its use combined with paramagnetic CEST agents characterized by a large separation of chemical shift values can be particularly beneficial. Another possibility, based on a postprocessing analysis, is to properly model the

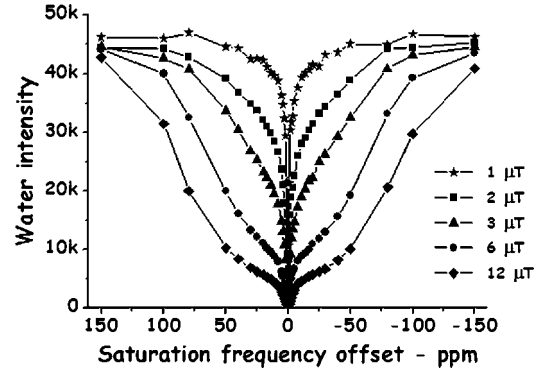

Figure 13. *In vivo* Z-spectra (7 T) of a mouse muscle at different B_2 amplitudes (from 1 to 12 μT). IWith increasing B_2 values, the MT component appears as a broad peak apparently centered at the same frequency of free water protons.

MT contribution, as nicely exemplified in a work recently published by Li et al.[189]

Concerning postprocessing analysis, novel modalities for enhancing the CEST contrast that are not merely based on the determination of the water signal intensity at a single frequency offset have been recently proposed.[190]

5. Challenges for Heteronuclear MR Imaging

The detection of a MR signal from a nuclear spin different from that of a proton may have the advantage of high contrast-to-noise ratios, as typically there is no signal from the tissue background. At the same time, two issues need to be addressed: (i) the necessity to superimpose the heteronuclear image to a standard proton image in order to spatially localize the origin of the contrast and (ii) the lower sensitivity of the heteronuclear detection with respect to the ^{1}H water signal. The latter point restricts the number of heteronuclei that can be imaged in clinical MRI to ^{19}F and hyperpolarized systems.

5.1. ^{19}F-Based Probes

The fluorine-19 isotope possesses several favorable NMR properties, including the nuclear spin of $^1/_2$ and the second highest receptivity value (0.83) after that of a proton, but the very low abundance (less than micromolar) of fluorine-containing compounds in living systems has ruled out any applicability of ^{19}F MRI to detect endogenous compounds. However, ^{19}F detection has been used in several biomedical research applications, including, among others, the study of tumor metabolism,[191] monitoring of tissue pO_2,[192] and imaging of the cardiovascular system.[193]

One can envisage several issues related to the *in vivo* translation of ^{19}F-MRI.

First of all, in close analogy to any heteronuclear imaging protocol, a conventional proton image needs to be coregistered, possibly in the same imaging session, in order to spatially localize the origin of the ^{19}F signal; this challenge has been fulfilled as double ^{1}H/^{19}F imaging coils are now available.

Next, as the method relies on the administration of ^{19}F-containing agents, it is necessary that sufficiently high local concentrations are attained in order to obtain a good signal(contrast)-to-noise ratio. Though same papers have proven the feasibility to visualize important biomarkers (e.g., β-amyloid plaques) using small molecules containing few (even only one) fluorine atoms,[194] most of the work carried out so far with the aim of developing more sensitive ^{19}F probes has dealt with nanosized agents loaded with a huge number of magnetically equivalent or pseudoequivalent ^{19}F atoms. Among them, perfluorocarbon nanoparticles (PFCs) have attracted a large amount of interest.[26] Most of the work on PFCs has been carried out by G. M. Lanza, S. Wickline, and co-workers, who demonstrated the great potential of this nanoplatform for molecular ^{19}F-MR imaging. One of the most important advantages of using ^{19}F (compared to proton) is the possibility to quantify with good accuracy the amount of agent accumulated in a given region of interest. In fact, the ^{19}F signal is much less affected by phenomena such as probe compartmentalization that, conversely, can seriously influence the water signal in conventional T_1 and T_2 weighted proton MR images. Relevant examples can be found in the literature illustrating the potential of ^{19}F-MRI protocols for detecting and quantifying cardiovascular abnormalities such as atherosclerotic plaques[109] or neo-angiogenesis events using PFCs suitably designed for targeting specific epitopes such as fibrin or integrins (Figure 14).[195]

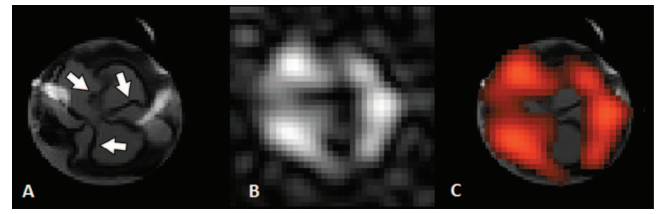

Figure 14. *Ex vivo* MR images (11.7 T) of rabbit aortic valves treated with $\alpha_v\beta_3$-integrin targeted PFC nanoparticles. (A) Proton image. (B) ^{19}F image. (C) False colored ^{19}F map overlaid on the proton image. Adapted with permission from ref 195. Copyright 2008 Biomed Central.

The detection threshold for the visualization of a ^{19}F signal from PFCs in a biological specimen has been estimated to be quite high (ca. 0.1 M at 4.7 T),[109] but considering the presence of ca. 10^8-10^9 fluorine atoms per particle, it is possible to detect up to nanomolar amounts of PFCs.

This approach has also been extended to cellular labeling. In 2007 Ahrens and co-workers described an *in vivo* imaging method for visualizing and quantifying a specific cell population.[196] T cells were *ex vivo* labeled with a perfluoropolyether nanoparticle (PEPE) tracer and then detected *in vivo* using ^{19}F MRI. The experiment selectively visualized only the labeled cells with no background, whereas the anatomical details were provided by a conventional proton image acquired in the same imaging session. Using a nonobese diabetic mouse, an established animal model of type 1 diabetes, the experiment demonstrated the early homing of diabetogenic T cells to the pancreas, and a computational algorithm provided T cell counts in the gland.

Obviously, another strategy for improving the contrast-to-noise ratio, but less feasible at the moment for clinical translations, is to increase the applied magnetic field strength.[197,198]

A potential drawback for detecting ^{19}F images is related to the low efficiency of T_1 relaxation processes that is detrimental for the temporal window of the experiment.

However, the T_1 can be properly shortened by designing protocols where the ^{19}F spins can be dipolarly relaxed by the presence of a paramagnetic species such as a Gd(III) complex.[199,200] In this case, the advantage can be 2-fold: in addition to shortening the total scan time for the ^{19}F detection, the probe can also be visualized by conventional proton MRI (as noted above, any ^{19}F-MRI protocol needs a coregistration of an anatomical proton image).

Nanotechnology offers important support for designing dual probes that may be used for these studies. For instance, PFCs can be easily engineered in order to contain tens of thousands of Gd(III) centers located on their surface. The paramagnetic centers can significantly improve the MRI/MRS properties of the ^{19}F probe, and a 4-fold enhancement in the magnetic relaxation rate of the ^{19}F nuclei accompanied with a 125% increase in the ^{19}F signal was observed *in vitro* and confirmed when the paramagnetic PFCs were targeted to human plasma clots.[201]

In addition, to better characterize the biodistribution and accumulation of the probe, the concomitant occurrence of ^{19}F spins and Gd centers may allow the design of innovative smart MRI ratiometric probes, as already described in section 2.7.[110]

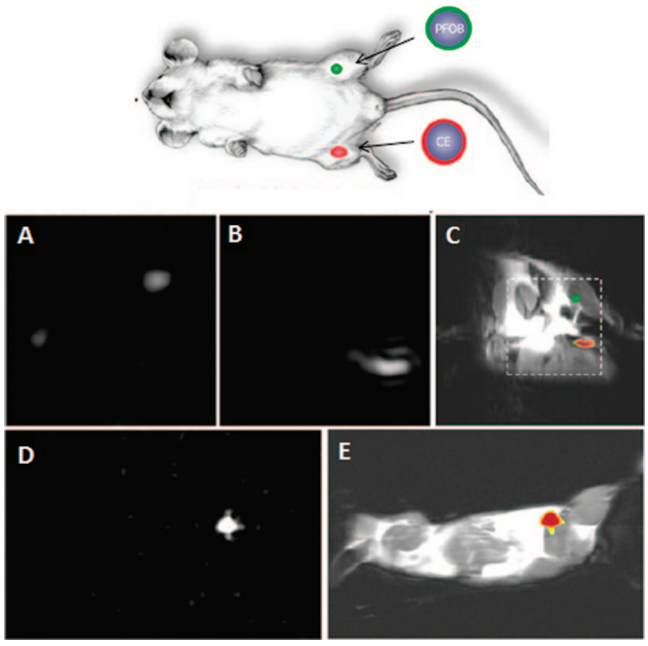

Figure 15. *In vivo* tracking of cells labeled with ^{19}F probes. Cells labeled with PFOB- (green) or CE- (red) PFC nanoparticles were injected into mouse thigh skeletal muscle. (A−C) The two cell populations can be singularly imaged at 11.7 T by exploiting the spectral differences of the ^{19}F labels (A, PFOB; B, CE). (C) Merged ^{19}F image overlaid on a conventional proton image for spatial localization. (D and E) Analogous experiment carried out on a clinical 1.5 T scanner. The images refer to CE-labeled cells. (D) ^{19}F image. (E) ^{19}F image overlaid on a proton image. Adapted with permission from ref 203. Copyright 2007 Federation of American Societies for Experimental Biology.

Another approach recently reported in the field of pH responsive ^{19}F MR probes is based on the design of paramagnetic lanthanide-based complexes acting as shift reagents for ^{19}F spins.[202] In this case, the ^{19}F resonance itself exhibits a pH dependent response and the presence of the paramagnetic center is exploited to improve the relaxation characteristics of the signal and to potentially allow a multiple detection of different probes' leveraging of the very large range window of chemical shift values accessible for ^{19}F nuclei. This favorable NMR property has also been used for developing multiplex ^{19}F-based MR imaging protocols.

In the field of MRI cell-tracking, another interesting example has been reported by G. M. Lanza/S. Wickline and co-workers, who labeled stem/progenitor cells with PFCs composed of two distinct lipophilic cores (perfluorooctylbromide and perfluoro-15-crown-5 ether).[203] Cells readily internalized the nanoparticles without the aid of adjunctive labeling techniques, and importantly, they remained functional *in vivo*. The sensitivity for detecting and imaging the labeled cells was defined at 11.7 T (research) and 1.5 T (clinical) MR scanners, and each cell population was imaged by exploiting the spectral signature of the ^{19}F label (Figure 15).

An analogous multiplex approach has been adopted in order to visualize gene expression by MRI either *in vitro*[204] or *in vivo* on a prostate cancer mouse model.[205]

Finally, the ^{19}F MRI signal of a fluorine-labeled molecule (fluoro-boron-*o*-phenylalanine, 19F-BPA) successfully used in boron neutron capture therapy (BNCT) has been used for assessing the *in vivo* biodistribution of the drug in a rat model of a brain tumor.[206]

6. Challenges for Hyperpolarized Probes

In spite of the great potentiality of magnetic resonance imaging (MRI) as a diagnostic tool and of magnetic resonance spectroscopy (MRS) as a useful technique to assess metabolic pathways, both of them suffer from the low sensitivity which is intrinsic in the NMR experiment. For this reason, the applications of MRI have been essentially restricted to ^{1}H (100% natural abundance, high γ value). Low γ heteronuclei have been used only for MRS,[207,208] but very long acquisition times are in this case necessary, and still only highly concentrated species can be detected.

Recently, the development of hyperpolarization techniques has opened the way to the use of heteronuclei without the need for long acquisition procedures. An hyperpolarized state is defined as a state in which the nuclear spin populations are altered with respect to the equilibrium value described by the Boltzmann equation. Since the signal intensity is proportional to the spin populations difference, hyperpolarization leads to an increase in the NMR signal intensity, which may reach values as high as 10^5. This can be exploited in the fast acquisition of high resolution MR images and spectra and allows us to use nuclei other than protons, allowing us to obtain images which are characterized by high signal-to-noise (S/N) ratios and free from background noise because of the low natural abundance of heteronuclei such as ^{13}C and ^{15}N.

Conversely to standard MRI contrast agents, based on paramagnetic systems, which act on the relaxation of water protons, and analogously to ^{19}F-containing compounds, hyperpolarized molecules are themselves the source of the NMR signal, and signal intensity and SNR linearly depend upon their concentration and polarization level. For this reason, a fundamental requisite for an hyperpolarized molecule to be used as an MRI/MRS contrast agent is the long relaxation time of the heteronucleus of interest. In fact, there must be a time long enough to acquire the image/spectrum before the relaxation processes re-establish the equilibrium spin populations, thus causing loss of signal. The low γ values that are typical of most heteronuclei cause themselves longer relaxation times with respect to protons; nevertheless, symmetrical environments and long distances from high γ nuclei (perdeuteration of the molecule is often pursued) should be preferred solutions, as these characteristics are effective in decreasing the CSA (chemical shift anisotropy) and dipolar contributions to relaxation, respectively.[209] Furthermore, small molecules are preferred, since their higher mobility in solution contributes to the maintenance of low relaxation rates.[210]

Four different methods have been proposed to produce hyperpolarized molecules: the "brute force" approach, optical pumping and spin exchange, dynamic nuclear polarization (DNP), and para-hydrogen induced polarization (PHIP).

6.1. Brute Force

The "brute force" approach consists of keeping the sample at very high magnetic field and ultralow temperature for a time sufficiently long to reach a new equilibrium distribution of the nuclei on the nuclear spin levels, according to the Boltzmann equation. The main issue of the method is the need for suitable "relaxation switches" due to the very low relaxation rates in the ultralow temperature range, in order to decrease the polarization time. These switches act as relaxation enhancers while the sample is at low temperature,

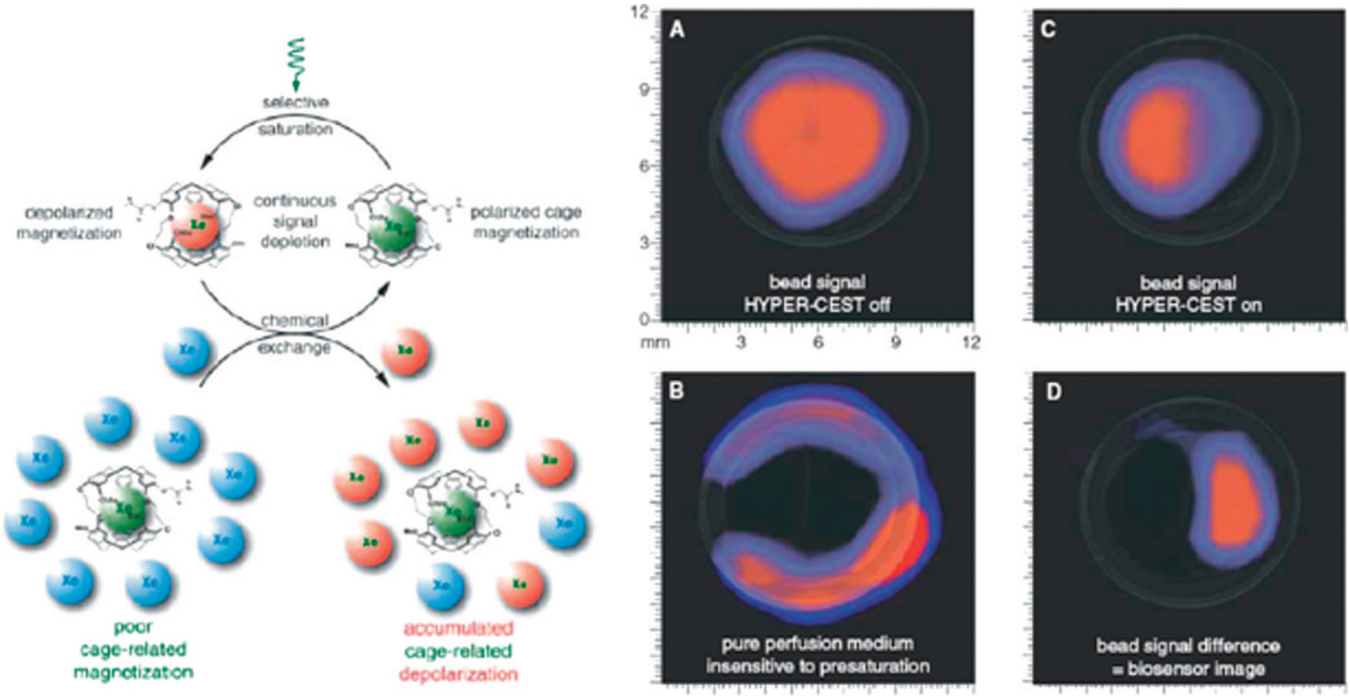

Figure 16. Left: HYPER-CEST scheme. Right: Molecular imaging of the Xe biosensor on avidin-agarose beads. In part D, the difference image of the two CSI data sets yields a molecular image of the Xe biosensor. Adapted with permission from ref 216. Copyright 2006 Advanced Science Serving Society.

but after polarization has been built in, they must be removed or "silenced". For example, paramagnetic molecular oxygen may be added to the sample and eliminated at the end of the hyperpolarization procedure by evaporation at low temperature. Another example is ^{3}He gas ($I = {}^1/_2$), which diffuses at very low temperature and promotes relaxation by dipolar interaction and may be replaced by the magnetically inert ^{4}He isotope after polarization has raised it to the desired level.[210] Actually, the "brute force" method has not found relevant applications due to difficulties in reaching the required very high magnetic field strengths and very low temperatures.

Furthermore, the relaxation switches may cause relaxation and polarization loss during the warming up of the sample if their removal, or silencing, is not complete.

6.2. Optical Pumping and Spin Exchange

Optical pumping and spin exchange is an hyperpolarization method which can be used to polarize noble gases (^{3}He and ^{129}Xe). A mixture of the noble gas and a vapor of an alkali-metal (in this case the method is defined as "spin-exchange optical pumping") or of metastable atoms (usually ^{3}He atoms; in this case it is named "metastability optical pumping") is irradiated with circularly polarized light from lasers at a suitable frequency. The angular momentum of the laser light is absorbed by the alkali or metastable atoms, and their polarization is then transferred to the noble gas atoms via "spin exchange" during the lifetime of Van-der-Waals molecules which are formed by interatomic collisions.[211,212] This method allows us to obtain very high polarization levels, which can be maintained for a long time due to the long relaxation times of ^{3}He and ^{129}Xe. However, the use of noble gases is limited to studies of the lungs and to some perfusion investigations.[211−215]

A very interesting application of hyperpolarized ^{129}Xe has been reported by Pines and co-workers.[216] It deals with a targeting procedure based on the use of a probe entrapping a ^{129}Xe atom in a molecular cage. The cage-encapsulated ^{129}Xe displays a resonance that is well shifted from that of free ^{129}Xe, and the two chemically different ^{129}Xe nuclei are involved in an exchange process on the NMR time scale. By irradiating the ^{129}Xe resonance of the entrapped Xe, a saturated magnetization is transferred to the signal of the free ^{129}Xe. This procedure has been dubbed HYPER-CEST, as it recalls the CEST (chemical exchange saturation transfer) protocol.

As a proof of concept, the procedure has been tested *in vitro* by using a ^{129}Xe biosensor consisting of ^{129}Xe entrapped in a criptophane-A cage linked through a spacer to a biotin unit. The ^{129}Xe biosensor binds avidin-agarose beads contained in one of the two compartments of a specifically designed flow system. The other compartment contained agarose beads not functionalized with avidin moieties. The application of the Hyper-CEST technique allowed us to precisely localize the ^{129}Xe biosensor in the phantom, in spite of the very low sensor concentration (2 μM) (Figure 16).

More recently, a ^{129}Xe biosensor specific for targeting the MHC (major hystocompatibility complex) protein has been prepared by using the criptophane-A Xe-entrapping cage, bound to the hemagglutinin (HA) peptide. The HYPER-CEST procedure was demonstrated to be effective for the detection of the ^{129}Xe biosensor bound to the protein in spite of the small difference in the chemical shifts of free and MHC-bound ^{129}Xe biosensors.[217]

6.3. Dynamic Nuclear Polarization (DNP)

Dynamic nuclear polarization (DNP) is probably the most versatile hyperpolarization method. In fact, in principle it allows hyperpolarization of every nucleus in every molecule, and for this reason, it is at the moment the method of choice for the production of hyperpolarized molecules which are currently under testing for imaging applications. The material

to be polarized is dissolved in a glass-forming solvent (glycerol, ethanol, or dimethylsulfoxide), or it can be used as it is if it forms a glassy structure when lowering the temperature. It is then doped with a stable radical species (usually a nitroxide or trytil derivative): glasslike structures are necessary in order to guarantee the highest homogeneity of the radical distribution in the solid. The sample is then placed into the magnetic field, brought to very low temperature (1−2 K), and irradiated with a proper microwave frequency, at or near the electron resonance frequency. Under these conditions, polarization transfer from electrons (whose polarization approaches 100% in this temperature range) to nuclei occurs via flip-flop transitions. The very unefficient nuclear relaxation in the solid ensures the maintenance of the nuclear spins alignment during the process.[218,219] After the polarization transfer has taken place, the rf is switched off, and the sample is raised above the liquid helium level and is rapidly dissolved in hot buffer still inside the magnetic field. This dissolution method allows us to rapidly reach body temperature without significant loss of polarization.[220] The sample is then injected into live animals or added to cells suspensions for MRI/MRS acquisitions.

Up to now, a number of biological substrates have been polarized by means of DNP. Among them, ^{15}N in urea,[220] carbazole,[221] amino acids,[222] and choline[223] and ^{89}Y in Y(III) chelates,[224] but none of these has found applications in MRI. At the moment, only ^{13}C has been used for *in vivo* MRI experiments, due to its higher sensitivity and to the availability of dedicated rf coils tuned at the ^{13}C frequency.

The most challenging application of hyperpolarized probes is their use for the assessment of metabolic pathways. Since abnormalities in cellular metabolism are primary indications of the passage from healthy to pathological states, it is of paramount importance to have the possibility for a direct, quantitative visualization of key metabolites' formation.[225−227]

Several ^{13}C-labeled substrates have been tested for hyperpolarization and metabolic applications. Hyperpolarized ^{13}C-lactate has been used to assess the activity of lactate dehydrogenase (LDH), which converts lactate into pyruvate. Multiple enzymatic steps, including the subsequent conversion of pyruvate to alanine and bicarbonate, have been evidenced.[228]

Hyperpolarized ^{13}C-glutamine has been used to assess the intramithocondrial activity of glutaminase in cultured human hepatocellular carcinoma cells by monitoring its conversion into glutamate.[229]

Hyperpolarized ^{13}C-labeled bicarbonate has been used to assess tissutal pH, which is an important parameter, since many pathological states, including tumors, are associated with pH changes. It has been shown that, upon injection of a solution of hyperpolarized ^{13}C-labeled bicarbonate, hyperpolarized carbon dioxide is rapidly formed by the action of carbonic anhydrase (CA) and can be detected by MRS. pH can thus be evaluated from ^{13}C MR measurements of the relative signal intensities of bicarbonate and carbon dioxide. By this method, it has been possible to measure tumor pH in live mice, confirming low intratumoral pH values (Figure 17).[230]

Hyperpolarized [1,4-^{13}C2]fumarate has been shown to be a sensitive marker for cellular necrosis: in fact, its transformation into [1,4-^{13}C2] malate, catalyzed by fumarase, is increased in tumor cells after treatment. This finding suggests the use of hyperpolarized fumarate as a positive marker of tumor response to treatment, in contrast to hyperpolarized

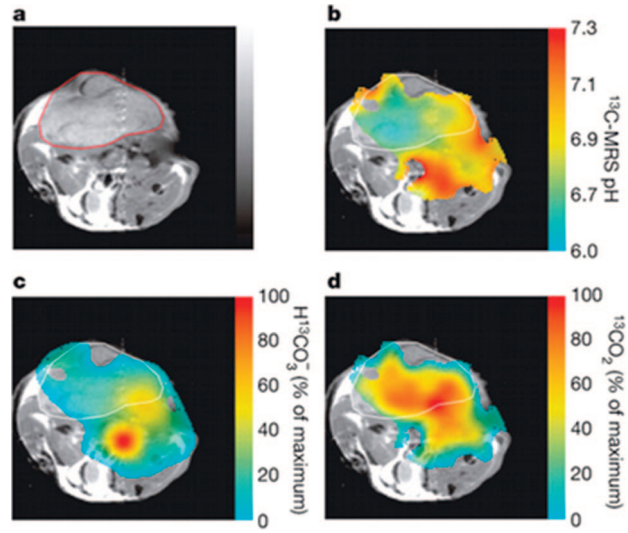

Figure 17. (a) Transverse ^{1}H MR image of a mouse with an EL4 tumor (outlined in red). (b) pH map calculated from the ratio of the $H^{13}CO_3^-$ (c) and $^{13}CO_2$ (d) voxel intensities in ^{13}C chemical shift images acquired 10 s after injection of 100 mM hyperpolarized $H^{13}CO_3^-$. Reprinted with permission from ref 230. Copyright 2008 Macmillan Publishers Ltd.

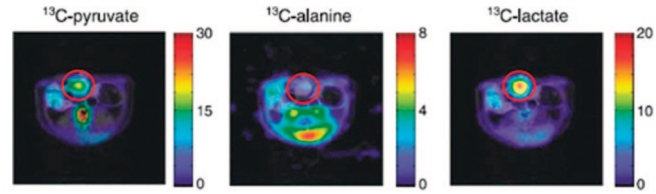

Figure 18. Images representing the intensity of ^{13}C-pyruvate, ^{13}C-alanine, and ^{13}C-lactate produced after injection of 1-^{13}C-pyruvate into a rat with a P22 tumor (outlined in red). Adapted with permission from ref 233. Copyright 2006 American Association for Cancer Research.

pyruvate, which is being considered as a negative marker (since its conversion to lactate is decreased after tumor treatment; see below).[231]

Real time alanine metabolism has been followed in healthy mice after injection of hyperpolarized ^{13}C-alanine, showing the feasibility of the use of hyperpolarized amino acids for the assessment of transaminase activity.[232]

The most studied molecule for metabolic investigations is at the moment ^{13}C-labeled pyruvate, hyperpolarized by a DNP procedure. Pyruvate is a key-molecule in major metabolic and catabolic pathways in mammalian cells. It is converted to lactate by the action of lactate dehydrogenase (LDH), to alanine by alanine transaminase (ALT), and to carbonate by pyruvate dehydrogenase (PDH) to a different extent depending on the status of the cells.

1-^{13}C-Hyperpolarized pyruvate has been used for tumor detection and stadiation, by exploiting the increased lactate production through LDH in tumor tissues. Murine lymphoma, P22 rat sarcoma, and adenocarcinoma of mice prostate have been studied by this method (Figure 18).[233−237]

Furthermore, the reduction of the conversion of pyruvate to lactate in tumors has been observed within 24 h of chemotherapy in the treatment of lymphoma-bearing mice,[238] suggesting that hyperpolarized 1-^{13}C-pyruvate may also find application in the evaluation of the response to therapeutic treatment. This result has been recently confirmed by comparing the response to treatment as measured by hyperpolarized 1-^{13}C-pyruvate MRI and by PET determination of

fluorodeoxyglucose (FDG). FDG uptake resulted to be a good reporter of the response to treatment at a shorter time with respect to 1-^{13}C-pyruvate, but after 24 h, the results were comparable for the two methodologies.[239]

Cardiac metabolism has also been assessed by means of metabolic imaging after injection of hyperpolarized 1-^{13}C-pyruvate both in isolated perfused rat hearts and *in vivo*. In this case it has been possible to differentiate healthy, ischemic, or postischemic tissue on the basis of the bicarbonate level in the myocardium, which is lower or absent in the areas where ischemia was present due to a decreased activity of pyruvate deyhdrogenase (PDH).[240−244]

Recently, cardiac metabolism has been investigated by means of hyperpolarized 2-^{13}C-pyruvate, affording some more information with respect to 1-^{13}C-pyruvate. In fact, in this case it has been possible to acquire simultaneous information about glycolysis (assessed by 2-^{13}C-lactate formation), PDH flux (assessed by 1-^{13}C-acetylcarnitine production), and the Krebs cycle (via the formation of 5-^{13}C-glutamate and 1-^{13}C-cytrate).[245]

Finally, liver metabolism is currently being investigated by means of hyperpolarized 1-^{13}C-pyruvate. In mice, the production of alanine by ALT has been shown to be sensitive to fasting. The use of hyperpolarized 1-^{13}C-pyruvate as a marker for ALT has been suggested as an alternative to the serum ALT test.[246] The ethanol metabolism has also been assessed by following the transformation of pyruvate to lactate in liver, which is increased after ethanol administration due to the increased NADH level associated with ethanol metabolism.[247]

6.4. para-Hydrogen Induced Polarization (PHIP)

In spite of its versatility, the DNP technique requires expensive technological devices and does not allow production of large quantities of hyperpolarized agents. Conversely, the hyperpolarization procedure based on para-hydrogen induced polarization (PHIP) is more demanding in terms of possible candidate substrates but has the advantages of minor complexity and cheapness. The hydrogen molecule exists as two different nuclear spin isomers: ortho-hydrogen (o-H_2), corresponding to a triply degenerate state ($S = 1$, 75% natural abundance), in which the two nuclear spins are parallel, and para-hydrogen (p-H_2), corresponding to a singlet state ($S = 0$, 25% abundance), in which the two nuclear spins are antiparallel. It is possible to enrich hydrogen in the para form at low temperature in the presence of a paramagnetic catalyst. The PHIP procedure is based on the chemical reaction of hydrogen enriched in the para form (commonly termed as para-hydrogen) with unsaturated substrates. The imbalance in the spin population of the para-hydrogen molecule is transferred to the product molecules, which result then transformed into hyperpolarized systems. The PHIP phenomenon has been recently reviewed.[248−252] In the hydrogenated molecule, polarization transfer to heteronuclei scalarly coupled with the hydrogen atoms deriving from the original para-hydrogen molecule can be implemented randomly by the application of a magnetic field cycle or selectively via special pulse sequences in which the time intervals between pulses are tailored on the molecule on the basis of the scalar coupling values.[253−259]

Clearly, in order to be hyperpolarized by PHIP, a molecule must contain an unsaturation in a position adjacent to the heteronucleus of interest. This limits the application of the PHIP procedure to unsaturated precursors of the molecules of interest, which in many cases are not available for biologically relevant substances.

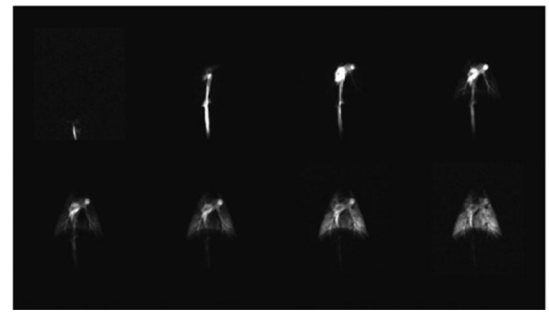

Figure 19. HP ^{13}C MRI angiograms depicting pulmonary blood flow, taken at 1-s intervals after injection of HP 2-hydroxyethyl propionate into a pig. Reprinted with permission from ref 265. Copyright 2007 Wiley & Sons.

It has been recently shown that para-hydrogen polarization can be transferred to molecules without chemical reaction when both the para-hydrogen and the substrate molecules reversibly interact on a metal center. This has been demonstrated by the detection of a good signal enhancement for the ^{15}N resonances of N-containing substrates reversibly coordinated to an Ir complex that has been added to a para-hydrogen molecule. The phenomenon has been named SABRE (signal amplification by reversible exchange)[260] and offers a novel, really interesting route to hyperpolarization via para-H_2 not involving substrate hydrogenation, as previously assumed.

For *in vivo* applications the catalyst used for para-hydrogenation and the organic solvent (present if the para-hydrogenation is not carried out in water) must be removed before injection. The catalyst (mainly cationic Rh(I) complexes, or Ir complexes in the SABRE case) may be removed by cation exchange and the solvent by spray-distillation. The fulfillment of these operations requires time, that is at the expense of the attainable signal intensity, as polarization decay occurs on the T_1 time scale. An alternative method consists of carrying out the para-hydrogenation reaction in an organic solvent not miscible with water and then quickly extracting the hyperpolarized water-soluble molecule by phase transfer.[261]

The first applications of PHIP-hyperpolarized molecules as ^{13}C-MRI probes were in the field of vascular imaging. Golman et al. reported the first angiographic image of a rat after injection of hyperpolarized ^{13}C-dimethylmaleate obtained by para-hydrogenation of ^{13}C-dimethylacetylenedicarboxylate in 2001.[262] Since then, a number of papers have appeared in the literature, reporting the use of hyperpolarized hydroxyethylpropionate (derived by para-hydrogenation of hydroxyethylacrylate) to obtain angiographic images of live animals (Figure 19).[263−265]

The fact that hyperpolarized nuclei in the administrated molecules are the direct signal sources and thus provide a direct relationship between the tracer concentration and the signal intensity can be exploited for the determination of perfusion parameters (cerebral blood flow, CBF, cerebral blood volume, CBV, and mean transit time, MTT), taking into consideration that in this case the polarization decay of the tracer produces an apparently faster decrease of the signal. This can be accounted for by suitably modifying the currently used Bolus Tracking Theory (which correlates the signal intensity with the contrast agent concentration in the tissue), as suggested by Johansson et al. Cerebral perfusion maps in

rats have been obtained by this method.[266] The fact that the polarization of the hyperpolarized tracer can be destroyed by applying a radiofrequency excitation has been exploited in the development of an alternative method, called bolus differentiation, which can also be used to perform tissues blood flow quantification. By this method, parametric maps for the assessment of renal cortical blood flow in rabbits have been obtained by using ^{13}C enriched 2-hydroxyethylpropionate polarized by PHIP.[267] Perfusion imaging with hyperpolarized ^{13}C contrast agents may find application for the attainment of high resolution perfusion pulmonary maps. Furthermore, it might be possible to study both ventilation and perfusion in real time by injecting simultaneously a ^{13}C and a ^{3}He hyperpolarized contrast agent.

Interventional endovascular MRI can also take advantage of the absence of a ^{13}C background signal when a ^{13}C hyperpolarized contrast agent is used. For example, a detailed study of the 3D reconstruction of a catheter moving along the aorta of a pig obtained by using 2-hydroxyethylpropionate obtained by PHIP as the hyperpolarized molecule has been reported.[268]

6.5. Use of Gd Contrast Agents with Hyperpolarized Substances

The distinction between intra- and extracellular metabolites originating from an injected hyperpolarized agent still remains an unsolved important issue to match with. It has been suggested that the distinction may be evidenced by combining hyperpolarized contrast agents and paramagnetic contrast agents.[269,270] In fact, since contrast agents are designed to not cross the cellular membrane, their effect on the relaxation of the hyperpolarized heteronucleus will be confined to the outer part of the cell, thus quenching the polarization of extracellular metabolites and not that of intracellular ones. The outer sphere effect of clinical paramagnetic Gd contrast agents (Omniscan, Magnevist, Dotarem, Gadovist) on the relaxation of heteronuclei has been reported for ^{13}C-formic acid and ^{13}C-glutamate[269] and for ^{13}C-glycine, ^{13}C-pyruvate, and ^{15}N-choline,[270] with variations among the different types of contrast agents being described in terms of distances between the heteronucleus of interest and Gd. The relaxation enhancement produced on the ^{15}N nucleus in ^{15}N-containing molecules has been exploited to demonstrate how the polarization can be destroyed after injection of a Gd contrast agent into an hyperpolarized solution, by using ^{15}N-tetramethylammonium as a model molecule.[270] Greater effects are expected to be observed when using Gd complexes of heptadentate ligands such as DO3A- and DO3A-like molecules, which are capable of binding the hyperpolarized molecule in the inner coordination sphere of Gd. The dramatic relaxation enhancements induced by this type of complexes has indeed been demonstrated by both ^{1}H and heteronuclear relaxation measurements on ^{13}C-lactate in the presence of the [Gd(DO3A)] class of complexes.[271]

An innovative approach for the detection of low concentrations of Gd(III) agents has been recently reported by van Heeswijk et al.[272] This method uses hyperpolarized ^{6}Li as the detectable signal, and it exploits a strong interaction between the metal ion and the negatively charged Gd-DOTP complex in order to shorten the T_1 of the ^{6}Li isotope, thus allowing a fast (and single-shot) contrast detection of the ^{6}Li signal in the presence of submicromolar amounts of the paramagnetic probe.

6.6. Issues with Hyperpolarized Agents

Two factors must be taken into account when performing imaging of hyperpolarized molecules: (i) polarization returns to its equilibrium value according to the relaxation time of the nucleus considered, and (ii) the application of rf pulses destroys magnetization. Consequently, pulse sequences must be designed in order to shorten the total acquisition time and low flip angles values must be used to preserve magnetization. In principle, any fast imaging sequence may be used.

The first papers about HP-MRI reported the use of RARE (rapid acquisition with relaxation enhancement), EPI (echo planar imaging), and trueFISP (fast imaging with steady state free precession) sequences, with trueFISP being the most used one because it enables us to recycle the transverse magnetization from one cycle to the next.[263,273] More recently, several papers dealing with CSI sequence optimization have appeared in the literature.[224−226,274] Sequences with gradient-refocusing, such as spiral imaging (SI), which uses a multiecho spiral acquisition to acquire both spatial and chemical shift information, and echo-planar spectroscopic imaging (EPSI), have been proposed for the simultaneous acquisition of the whole spectrum. Sequences based on rf refocusing can also be used; for example, a double spin−echo sequence has been proposed, which is characterized by insensitivity to calibration of the transmitter gain, formation of a spin−echo that affords high-quality spectral information, and a small effective tip angle which preserves the magnetization.[226] The use of multiband, variable flip angle rf pulses instead of constant flip angle sequences has been shown to increase the SNR in CSI and to allow longer time courses for metabolic products.[227] Since the image quality depends on the resolution of the metabolite resonances, least-squares-based image reconstruction methods have been proposed to improve the spectral quality. In this case, a number of images are acquired at different echo times, and reconstruction is obtained by analyzing the differences in signal behavior between peaks with different chemical shifts.[225,274]

7. Concluding Remarks

Molecular imaging is a new science that will have a tremendous impact in understanding biology and in the development of innovative diagnostic tools for early diagnoses and monitoring therapeutic treatments. In the first stage of its enrollment, it has relied massively on PET/SPECT and optical imaging technologies because of the superior sensitivity of their tracers. In the long-term, MRI/MRS approaches may recover a central role, provided that further sensitivity improvement will be attained. As discussed in this survey, there are several routes to tackle these issues and the promises are very positive thanks to the multinuclear, multiparametric characteristics of the NMR experiment. Along the way to improve the competitive aspect of MRI/MRS with respect to the other imaging modalities, there is not only a need to endow the probes with higher sensitivity and targeting specificity. Very important will be the development of frequency-encoding contrast agents in order to make the MRI approach the one that allows the multidetection of different reporting agents in the same image. As molecular imaging is the evolution of biologist *in vitro* work that has revolutionized the way living cells and intact tissues were investigated, MRI multiplex-visualization of biological processes appears to be a key task for the forthcoming years for an efficient

translation of such outstanding achievements. Moreover, new avenues for MRI/MRS probes will have to be undertaken to face the technological advances, for instance in the field of dual-modality scanners that will soon be available to the clinical practice.

Simultaneous MRI-PET acquisition will have great advantages if chemists will be able to develop agents that exploit the complementarities between the two modalities. Finally, much attention will have to be devoted to the development of MRI-guided therapies. Upon entering the era of personalized medicine, new therapeutic approaches will be undertaken in order to deliver drugs at their sites of action, limiting the problems associated with their systemic toxicity. Merging MRI and nanotechnology appears to be the right way to design "smart", targeted nanocarriers, whereas proceeding to drug release at the diseased cells provides the imaging platform to detect in real time the effect of the drug itself. It sounds like science-fiction, but it is just around the corner.

8. Acknowledgments

The authors would like to thank Bracco Imaging SpA (Milano, Italy) for the longstanding collaboration. Financial support from Regional government (Nano-IGT project, Converging Technologies CIPE 2007), MIUR (FIRB RBIP06293N and PRIN 2007W7M4NF projects), EU-FP6-projects DiMI (Diagnostic Molecular Imaging: LSHB-CT-2005-512146), MEDITRANS (Targeted Delivery of Nanomedicine: NMP4-CT-2006-026668), and EU-FP7 project ENCITE (European Network for Cell Imaging and Tracking Expertise: 201842) is gratefully acknowledged. EU-COST D38 Action (metal-based systems for molecular imaging applications) is also acknowledged.

9. References

(1) Weissleder, R.; Mahmood, U. *Radiology* **2001**, *219*, 316.
(2) Hoult, D. I.; Lauterbur, P. C. *J. Magn. Reson.* **1979**, *34*, 425.
(3) Laniado, M.; Weinmann, H. J.; Schorner, W.; Felix, R.; Speck, U. *Physiol. Chem. Phys. Med. NMR* **1984**, *16*, 157.
(4) Lauffer, R. B. *Chem. Rev.* **1987**, *87*, 901.
(5) Aime, S.; Delli Castelli, D.; Geninatti Crich, S.; Gianolio, E.; Terreno, E. *Acc. Chem. Res.* **2009**, *42*, 822.
(6) Caravan, P. *Acc. Chem. Res.* **2009**, *42*, 851.
(7) Werner, E. J.; Datta, A.; Jocher, C. J.; Raymond, K. N. *Angew. Chem., Int. Ed.* **2008**, *47*, 8568.
(8) Hermann, P.; Kotek, J.; Kubicek, V.; Lukes, I. *Dalton Trans.* **2008**, *23*, 3027.
(9) Caravan, P.; Ellison, J. J.; McMurry, T. J.; Lauffer, R. B. *Chem. Rev.* **1999**, *99*, 2293.
(10) Geraldes, C. F. G. C.; Laurent, S. *Contrast Media Mol. Imaging* **2009**, *4*, 1.
(11) Aime, S.; Geninatti Crich, S.; Gianolio, E.; Giovenzana, G. B.; Tei, L.; Terreno, E. *Coord. Chem. Rev.* **2006**, *250*, 1562.
(12) Aime, S.; Botta, M.; Terreno, E. *Adv. Inorg. Chem.* **2005**, *57*, 173.
(13) Botta, M. *Eur. J. Inorg. Chem.* **2000**, *3*, 399.
(14) Corot, C.; Robert, P.; Idée, J. M.; Port, M. *Adv. Drug Delivery Rev.* **2006**, *58*, 1471.
(15) Laurent, S.; Forge, D.; Port, M.; Roch, A.; Robic, C.; Vander Elst, L.; Muller, R. N. *Chem. Rev.* **2008**, *108*, 2064.
(16) Gupta, A. K.; Naregalkar, R. R.; Vaidya, V. D.; Gupta, M. *Nanomedicine* **2007**, *2*, 23.
(17) Shubayev, V.; Pisanic, T. R.; Jin, S. *Adv. Drug. Delivery Rev.* **2009**, *61*, 467.
(18) Xie, J.; Huang, J.; Li, X.; Sun, S.; Chen, X. *Curr. Med. Chem.* **2009**, *16*, 1278.
(19) Gao, J.; Gu, H.; Xu, B. *Acc. Chem. Res.* **2009**, *42*, 1097.
(20) Bulte, J. W. M. *Am. J. Roentgenology* **2009**, *193*, 314.
(21) Ward, K. M.; Aletras, A. H.; Balaban, R. S. *J. Magn. Reson.* **2000**, *143*, 79.
(22) Zhou, J.; van Zijl, P. C. M. *Prog. NMR Spectrosc.* **2006**, *48*, 109.
(23) Woods, M.; Woessner, D. E.; Sherry, A. D. *Chem. Soc. Rev.* **2006**, *35*, 500.
(24) Delli Castelli, D.; Gianolio, E.; Geninatti Crich, S.; Terreno, E.; Aime, S. *Coord. Chem. Rev.* **2008**, *252*, 2424.
(25) Zhang, S.; Merritt, M.; Woessner, D. E.; Lenkinski, R. E.; Sherry, A. D. *Acc. Chem. Res.* **2003**, *36*, 783.
(26) Lanza, G. M.; Winter, P. M.; Neubauer, A. M.; Caruthers, S. D.; Hockett, F. D.; Wickline, S. A. *Curr. Top. Dev. Biol.* **2005**, *70*, 57.
(27) Viale, A.; Reineri, F.; Santelia, D.; Cerutti, E.; Ellena, S.; Gobetto, R.; Aime, S. Q. J. *Nucl. Med. Mol. Imaging* **2009**, *53*, 604.
(28) Bloembergen, N.; Morgan, L. O. *J. Chem. Phys.* **1961**, *34*, 842.
(29) Aime, S.; Barge, A.; Botta, M.; Casnati, A.; Fragai, M.; Luchinat, C.; Ungaro, R. *Angew. Chem., Int. Ed.* **2001**, *40*, 4737.
(30) Avedano, S.; Tei, L.; Lombardi, A.; Giovenzana, G. B.; Aime, S.; Longo, D.; Botta, M. *Chem. Commun.* **2007**, 4726.
(31) Toth, E.; Pubanz, D.; Vauthey, S.; Helm, L.; Merbach, A. E. *Chem.—Eur. J.* **1996**, *2*, 1607.
(32) Rudovsky, J.; Botta, M.; Hermann, P.; Hardcastle, K. I.; Lukes, I.; Aime, S. *Bioconjugate Chem.* **2006**, *17*, 975.
(33) Nicolle, G. M.; Tóth, É.; Eisenwiener, K. P.; Mäcke, H. R.; Merbach, A. E. *J. Biol. Inorg. Chem.* **2002**, *7*, 757.
(34) Carniato, F.; Tei, L.; Dastru, W.; Marchese, L.; Botta, M. *Chem. Commun.* **2009**, 1246.
(35) Yerly, F.; Hardcastle, K. I.; Helm, L.; Aime, S.; Botta, M.; Merbach, A. E. *Chem.—Eur. J.* **2002**, *8*, 1031.
(36) Casali, C.; Janier, M.; Canet, E.; Obadia, J. F.; Benderbous, S.; Corot, C.; Revel, D. *Acad. Radiol.* **1998**, *5*, S214.
(37) Rohrer, M.; Bauer, H.; Mintorovitch, J.; Requardt, M.; Weinmann, H. J. *Invest. Radiol.* **2005**, *40*, 715.
(38) Zhang, Z.; Greenfield, M. T.; Spiller, M.; McMurry, T. J.; Lauffer, R. B.; Caravan, P. *Angew. Chem., Int. Ed.* **2005**, *44*, 6766.
(39) Aime, S.; Botta, M.; Fedeli, F.; Gianolio, E.; Terreno, E.; Anelli, P. L. *Chem.—Eur. J.* **2001**, *7*, 5262.
(40) Port, M.; Meyer, D.; Bonnemain, B.; Corot, C.; Schaefer, M.; Rousseaux, O.; Simonot, C.; Bourrinet, P.; Benderbous, S.; Dencausse, A.; Devoldere, L. *Magn. Reson. Mater. Phys.* **1999**, *8*, 172.
(41) Port, M.; Corot, C.; Rousseaux, O.; Raynal, I.; Devoldere, L.; Ide'e, J. M.; Dencausse, A.; Le Greneur, S.; Simonot, C.; Meyer, D. *Magn. Reson. Mater. Phys.* **2001**, *12*, 121.
(42) Fulton, D. A.; O'Halloran, M.; Parker, D.; Senanayake, K.; Botta, M.; Aime, S. *Chem. Commun.* **2005**, 474.
(43) Jacques, V.; Desreux, J. F. *Top. Curr. Chem.* **2002**, *221*, 123.
(44) Livramento, J. B.; Toth, E.; Sour, A.; Borel, A.; Merbach, A. E.; Ruloff, R. *Angew. Chem., Int. Ed.* **2005**, *44*, 1480.
(45) Livramento, J. B.; Weidensteiner, C.; Prata, M. I. M.; Allegrini, P. R.; Geraldes, C. F. G. C.; Helm, L.; Kneuer, R.; Merbach, A. E.; Santos, A. C.; Schmidt, P.; Toth, E. *Contrast Media Mol. Imaging* **2006**, *1*, 30.
(46) Livramento, J. B.; Helm, L.; Sour, A.; O'Neil, C.; Merbach, A. E.; Toth, E. *Dalton Trans.* **2008**, 1195.
(47) Livramento, J. B.; Sour, A.; Borel, A.; Merbach, A. E.; Toth, E. *Chem.—Eur. J.* **2006**, *12*, 989. Cossy, C.; Helm, L.; Powell, D. H.; Merbach, A. E. *New J. Chem.* **1995**, *19*, 27.
(48) Laus, S.; Ruloff, R.; Toth, E.; Merbach, A. E. *Chem.—Eur. J.* **2003**, *9*, 3555.
(49) Kotek, J.; Lebduskova, P.; Hermann, P.; Vander Elst, L.; Muller, R. N.; Geraldes, C. F. G. C.; Maschmeyer, T.; Lukes, I.; Peters, J. A. *Chem.—Eur. J.* **2003**, *9*, 5899.
(50) Aime, S.; Gianolio, E.; Longo, D.; Pagliarin, R.; Lovazzano, C.; Sisti, M. *ChemBioChem* **2005**, *6*, 818.
(51) Tei, L.; Botta, M.; Lovazzano, C.; Barge, A.; Milone, L.; Aime, S. *Magn. Reson. Chem.* **2008**, *46*, S86.
(52) Jaszberenyi, Z.; Sour, A.; Toth, E.; Benmelouka, M.; Merbach, A. E. *Dalton Trans.* **2005**, 2713.
(53) Tei, L.; Gugliotta, G.; Baranyai, Z.; Botta, M. *Dalton Trans.* **2009**, 9712.
(54) Aime, S.; Chiaussa, M.; Digilio, G.; Gianolio, E.; Terreno, E. *J. Biol. Inorg. Chem.* **1999**, *4*, 766.
(55) Aime, S.; Botta, M.; Garino, E.; Geninatti Crich, S.; Giovenzana, G. B.; Pagliarin, R.; Palmisano, G.; Sisti, M. *Chem.—Eur. J.* **2006**, *6*, 2609.
(56) Zech, S. G.; Eldredge, H. B.; Lowe, M. P.; Caravan, P. *Inorg. Chem.* **2007**, *46*, 3576.
(57) Baranyai, Z.; Gianolio, E.; Ramalingam, K.; Swenson, R.; Ranganathan, R.; Brücher, E.; Aime, S. *Contrast Media Mol. Imaging* **2007**, *2*, 94.
(58) Aime, S.; Gianolio, E.; Terreno, E.; Giovenzana, G. B.; Pagliarin, R.; Sisti, M.; Palmisano, G.; Botta, M.; Lowe, M. P.; Parker, D. *J. Biol. Inorg. Chem.* **2000**, *5*, 488.
(59) Aime, S.; D'Amelio, N.; Fragai, M.; Lee, Y.-M.; Luchinat, C.; Terreno, E.; Valensin, G. *J. Biol. Inorg. Chem.* **2002**, *7*, 617.

(60) Aime, S.; Botta, M.; Geninatti Crich, S.; Giovenzana, G. B.; Pagliarin, R.; Piccinini, M.; Sisti, M.; Terreno, E. *J. Biol. Inorg. Chem.* **1997**, *2*, 470.
(61) Aime, S.; Anelli, P. L.; Botta, M.; Brocchetta, M.; Canton, S.; Fedeli, F.; Gianolio, E.; Terreno, E. *J. Biol. Inorg. Chem.* **2002**, *7*, 58.
(62) Caravan, P. *Acc. Chem. Res.* **2009**, *42*, 851.
(63) Kim, W. D.; Kiefer, G. E.; Maton, F.; McMillan, K.; Muller, R. N.; Sherry, A. D. *Inorg. Chem.* **1995**, *34*, 2233.
(64) Aime, S.; Botta, M.; Geninatti Crich, S.; Giovenzana, G. B.; Jommi, G.; Pagliarin, R.; Sisti, M. *Inorg. Chem.* **1997**, *36*, 2992.
(65) Port, M.; Raynal, I.; Vander Elst, L.; Muller, R. N.; Dioury, F.; Ferroud, C.; Guy, A. *Contrast Media Mol. Imaging* **2006**, *1*, 121.
(66) Tircso, G.; Benyo, E. T.; Suh, E. H.; Jurek, P.; Kiefer, G. E.; Sherry, A. D.; Kovacs, Z. *Bioconjugate Chem.* **2009**, *20*, 565.
(67) Aime, S.; Calabi, L.; Cavallotti, C.; Gianolio, E.; Giovenzana, G. B.; Losi, P.; Maiocchi, A.; Palmisano, G.; Sisti, M. *Inorg. Chem.* **2004**, *43*, 7588.
(68) Elemento, E. M.; Parker, D.; Aime, S.; Gianolio, E.; Lattuada, L. *Org. Biomol. Chem.* **2009**, *7*, 1120.
(69) Gugliotta, G.; Botta, M.; Giovenzana, G. B.; Tei, L. *Bioorg. Med. Chem. Lett.* **2009**, *19*, 3442.
(70) Hajela, S.; Botta, M.; Giraudo, S.; Xu, J. D.; Raymond, K. N.; Aime, S. *J. Am. Chem. Soc.* **2000**, *122*, 11228.
(71) Thompson, M. K.; Botta, M.; Nicolle, G.; Helm, L.; Aime, S.; Merbach, A. E.; Raymond, K. N. *J. Am. Chem. Soc.* **2003**, *125*, 14274.
(72) Thompson, M. K.; Misselwitz, B.; Tso, L. S.; Doble, D. M. J.; Schmitt-Willich, H.; Raymond, K. N. *J. Med. Chem.* **2005**, *48*, 3874.
(73) Datta, A.; Raymond, K. N. *Acc. Chem. Res.* **2009**, *42*, 938.
(74) Werner, E. J.; Avedano, S.; Botta, M.; Hay, B. P.; Moore, E. G.; Aime, S.; Raymond, K. N. *J. Am. Chem. Soc.* **2007**, *129*, 1870.
(75) Gianolio, E.; Giovenzana, G. B.; Longo, D.; Longo, I.; Menegotto, I.; Aime, S. *Chem.—Eur. J.* **2007**, *13*, 5785.
(76) Geninatti Crich, S.; Lanzardo, S.; Alberti, D.; Belfiore, S.; Ciampa, A.; Giovenzana, G. B.; Lovazzano, C.; Pagliarin, R.; Aime, S. *Neoplasia* **2007**, *9*, 1046.
(77) Pierre, V. C.; Botta, M.; Raymond, K. N. *J. Am. Chem. Soc.* **2005**, *127*, 504.
(78) Datta, A.; Hooker, J. M.; Botta, M.; Francis, M. B.; Aime, S.; Raymond, K. N. *J. Am. Chem. Soc.* **2008**, *130*, 2546.
(79) Longmire, M.; Choyke, P. L.; Kobayashi, H. *Curr. Top. Med. Chem.* **2008**, *8*, 1180.
(80) Accardo, A.; Tesauro, D.; Aloj, L.; Pedone, C.; Morelli, G. *Coord. Chem. Rev.* **2009**, *253*, 2193.
(81) Mulder, W. J. M.; Strijkers, G. J.; Van Tilborg, G. A. F.; Cormode, D. P.; Fayad, Z. A.; Nicolay, K. *Acc. Chem. Res.* **2009**, *42*, 904.
(82) Sitharaman, B.; Wilson, L. J. *J. Biomed. Nanotechnol.* **2007**, *3*, 342.
(83) Na, H. B.; Hyeon, T. *J. Mater. Chem.* **2009**, *19*, 6267.
(84) Aime, S.; Frullano, L.; Geninatti Crich, S. *Angew. Chem., Int. Ed.* **2002**, *41*, 1017.
(85) Vasalatiy, O.; Zhao, P.; Zhang, S.; Aime, S.; Sherry, A. D. *Contrast Media Mol. Imaging* **2006**, *1*, 10.
(86) Delli Castelli, D.; Gianolio, E.; Geninatti Crich, S.; Terreno, E.; Aime, S. *Coord. Chem. Rev.* **2008**, *252*, 2424.
(87) Geninatti Crich, S.; Bussolati, B.; Tei, L.; Grange, C.; Esposito, G.; Lanzardo, S.; Camussi, G.; Aime, S. *Cancer Res.* **2006**, *66*, 9196.
(88) Ferenc, K. K.; Geninatti Crich, S.; Aime, S. *Angew. Chem., Int. Ed.* **2010**, *49*, 612.
(89) Sitharaman, B.; Kissell, K. R.; Hartman, K. B.; Tran, L. A.; Baikalov, A.; Rusakova, I.; Sun, Y.; Khant, H. A.; Ludtke, S. J.; Chiu, W.; Laus, S.; Toth, E.; Helm, L.; Merbach, A. E.; Wilson, L. J. *Chem. Commun.* **2005**, 3915.
(90) Pautler, R. G. *Methods Mol. Med.* **2006**, *124*, 365.
(91) Broome, D. R. *Eur. J. Radiol.* **2008**, *66*, 230.
(92) Toft, K. G.; Hustvedt, S. O.; Grant, D.; Martinsen, I.; Gordon, P. B.; Friisk, G. A.; Korsmo, A. J.; Skotland, T. *Acta Radiol.* **1997**, *38*, 677.
(93) Na, H. B.; Lee, J. H.; An, K.; Park, Y.; Park, M.; Lee, I. S.; Nam, D.-H.; Kim, S. T.; Kim, S.-H.; Kim, S.-W.; Lim, K.-H.; Kim, K.-S.; Kim, S.-O.; Hyeon, T. *Angew. Chem., Int. Ed.* **2007**, *46*, 5397.
(94) Gilad, A. A.; Walczak, P.; McMahon, M. T.; Na, H. B.; Lee, J. H.; An, K.; Hyeon, T.; van Zijl, P. C. M.; Bulte, J. W. M. *Magn. Reson. Med.* **2008**, *60*, 1.
(95) Shin, J.; Anisur, R. M.; Ko, M. K.; Im, G. H.; Lee, J. H.; Lee, I. S. *Angew. Chem., Int. Ed.* **2009**, *48*, 321.
(96) Pan, D.; Senpan, A.; Caruthers, S. D.; Williams, T. A.; Scott, M. J.; Gaffney, P. J.; Wickline, S. A.; Lanza, G. M. *Chem. Commun.* **2009**, 3234.
(97) Alford, J. K.; Rutt, B. K.; Scholl, T. J.; Handler, W. B.; Chronik, B. A. *Magn. Reson. Med.* **2009**, *61*, 796.
(98) Lurie, D. J.; Foster, M. A.; Yeung, D.; Hutchison, J. M. S. *Phys. Med. Biol.* **1998**, *43*, 1877.
(99) Louie, A. Y.; Huber, M. M.; Ahrens, E. T.; Rothbacher, U.; Moats, R.; Jacobs, R. E.; Fraser, S. E.; Meade, T. J. *Nat. Biotechnol.* **2000**, *18*, 321.
(100) Urbanczyk-Pearson, L. M.; Femia, F. J.; Smith, J.; Parigi, G.; Duimstra, J. A.; Eckermann, A. L.; Luchinat, C.; Meade, T. J. *Inorg. Chem.* **2008**, *47*, 56.
(101) Nahrendorf, M.; Sosnovik, D.; Chen, J. W.; Panizzi, P.; Figueiredo, J. L.; Aikawa, E.; Libby, P.; Swirski, F. K.; Weissleder, R. *Circulation* **2008**, *117*, 1153.
(102) Breckwoldt, M. O.; Chen, J. W.; Stangenberg, L.; Aikawa, E.; Rodriguez, E.; Qiu, S.; Moskowitz, M. A.; Weissleder, R. *Proc. Natl. Acad. Sci. U.S.A.* **2008**, *105*, 18584.
(103) Chen, J. W.; Breckwoldt, M. O.; Aikawa, E.; Chiang, G.; Weissleder, R. *Brain* **2008**, *131*, 1123.
(104) Rodriguez, E.; Nilges, M.; Weissleder, R.; Chen, J. W. *J. Am. Chem. Soc.* **2010**, *132*, 168.
(105) Raghunand, N.; Howison, C.; Sherry, A. D.; Zhang, S.; Gillies, R. J. *Magn. Reson. Med.* **2003**, *49*, 249.
(106) Garcia-Martin, M. L.; Martinez, G. V.; Raghunand, N.; Sherry, A. D.; Zhang, S.; Gillies, R. J. *Magn. Reson. Med.* **2006**, *55*, 309.
(107) Aime, S.; Fedeli, F.; Sanino, A.; Terreno, E. *J. Am. Chem. Soc.* **2006**, *128*, 11326.
(108) Terreno, E.; Delli Castelli, D.; Cabella, C.; Dastrù, W.; Sanino, A.; Stancanello, J.; Tei, L.; Aime, S. *Chem. Biodiversity* **2008**, *5*, 1901.
(109) Morawski, A. M.; Winter, P. M.; Yu, X.; Fuhrhop, R. W.; Scott, M. J.; Hockett, F.; Robertson, J. D.; Gaffney, P. J.; Lanza, G. M.; Wickline, S. A. *Magn. Reson. Med.* **2004**, *52*, 1255.
(110) Gianolio, E.; Napolitano, R.; Fedeli, F.; Arena, F.; Aime, S. *Chem. Commun.* **2009**, 6044.
(111) De Leon-Rodriguez, L. M.; Lubag, A. J.; Malloy, C. R.; Martinez, G. V.; Gillies, R. J.; Sherry, A. D. *Acc. Chem. Res.* **2009**, *42*, 948.
(112) Ali, M. M.; Woods, M.; Caravan, P.; Opina, A. C.; Spiller, M.; Fettinger, J. C.; Sherry, A. D. *Chem.—Eur. J.* **2008**, *14*, 7250.
(113) Aime, S.; Nano, R.; Grandi, M. *Invest. Radiol.* **1888**, *23*, S267.
(114) Vander Elst, L.; Zhang, S.; Sherry, A. D.; Laurent, S.; Botteman, F.; Muller, R. N. *Acad. Radiol.* **2002**, *9*, S297.
(115) Rabenstein, D. L.; Fan, S. *Anal. Chem.* **1986**, *58*, 3178.
(116) Ronen, I.; Merkle, H.; Ugurbil, K.; Navon, G. *Proc. Natl. Acad. Sci. U.S.A.* **1998**, *95*, 12934.
(117) Shapiro, E. M.; Skrtic, S.; Koretsky, A. P. *Magn. Reson. Med.* **2005**, *53*, 329.
(118) Shapiro, E. M.; Sharer, K.; Skrtic, S.; Koretsky, A. P. *Magn. Reson. Med.* **2006**, *55*, 242.
(119) McAteer, M. A.; Akhtar, A. M.; von zur Muhlen, C.; Choudhury, R. P. *Atherosclerosis* **2010**, *209*, 18.
(120) Gupta, A. J.; Gupta, M. *Biomaterials* **2005**, *26*, 3995.
(121) De Gennes, P. G. *Macromolecules* **1980**, *13*, 1069.
(122) Mornet, S.; Vasseur, S.; Grasset, F.; Duguet, E. *J. Mater. Chem.* **2004**, *14*, 2.
(123) Roger, J.; Pons, J. N.; Massart, R. *Eur. J. Solid State Inorg. Chem.* **1989**, *26*, 475.
(124) Fauconnier, N.; Bee, A.; Roger, J.; Pons, J. N. *Prog. Colloid Polym. Sci.* **1996**, *100*, 212.
(125) Fauconnier, N.; Pons, J. N.; Roger, J.; Bee, A. *J. Colloid Interface Sci.* **1997**, *194*, 427.
(126) Fauconnier, N.; Bee, A.; Roger, J.; Pons, J. N. *J. Mol. Liq.* **1999**, *83*, 233.
(127) Cunningham, C. H.; Arai, T.; Yang, P. C.; McConnell, M. V.; Pauly, J. M.; Conolly, S. M. *Magn. Reson. Med.* **2005**, *53*, 999.
(128) Suzuki, Y.; Cunningham, C. H.; Noguchi, K.; Chen, I. Y.; Weissman, I. L.; Yeung, A. C.; Robbins, R. C.; Yang, P. C. *Magn. Reson. Med.* **2008**, *60*, 1269.
(129) Stuber, M.; Gilson, W. D.; Schar, M.; Kedziorek, D. A.; Hofmann, L. V.; Shah, S.; Vonken, E. J.; Bulte, J. W. M.; Kraitchman, D. L. *Magn. Reson. Med.* **2007**, *58*, 1072.
(130) Korosoglou, G.; Weiss, R. G.; Kedziorek, D. A.; Walczak, P.; Gilson, W. D.; Schar, M.; Sosnovik, D. E.; Kraitchman, D. L.; Boston, R. C.; Bulte, J. W. M.; Weissleder, R.; Stuber, M. *J. Am. Coll. Cardiol.* **2008**, *52*, 483.
(131) Senpan, A.; Caruthers, S.; Rhee, I.; Mauro, N.; Pan, D.; Hu, G.; Scott, M.; Fuhrop, R.; Gaffney, P.; Wickline, S.; Lanza, G. *ACS Nano* **2009**, *3*, 3917.
(132) Modo, M.; Hoehn, M.; Bulte, J. W. *Mol. Imaging* **2005**, *4*, 143.
(133) Emerit, J. C.; Beaumont, C.; Trivin, F. *Biomed. Pharmacother.* **2001**, *55*, 333.
(134) Wang, F. H.; Lee, I. H.; Holmström, N.; Yoshitake, T.; Kim, D. K.; Muhammed, M.; Frisen, J.; Olson, L.; Spenger, C.; Kehr, J. *Nanotechnology* **2006**, *17*, 1911.
(135) Niemeyer, C. M.; Ceyhan, B. *Angew. Chem., Int. Ed.* **2001**, *40*, 3685.
(136) Sosnovik, D. E.; Nahrendorf, M.; Panizzi, P.; Matsui, T.; Aikawa, E.; Dai, G. P.; Li, L.; Reynolds, F.; Dorn, G. W.; Weissleder, R.; Josephson, L.; Rosenzweig, A. *Circ. Cardiovasc. Imaging* **2009**, *2*, 460.

(137) Sosnovik, D. E.; Nahrendorf, M.; Weissleder, R. *Basic Res. Cardiol.* **2008**, *103*, 122.
(138) Martina, M.-S.; Fortin, J.-P.; Menager, C.; Clement, O.; Barratt, G.; Grabielle-Madelmont, C.; Gazeau, F.; Cabuil, V.; Lesieur, S. *J. Am. Chem. Soc.* **2005**, *127*, 10676.
(139) Huber, D. L. *Small* **2005**, *1*, 482.
(140) Polyak, B.; Friedman, G. *Expert Opin. Drug Delivery* **2009**, *6*, 53.
(141) Shubayev, V. I.; Pisanic, T. R., II; Jin, S. *Adv. Drug Delivery Rev.* **2009**, *61*, 467.
(142) Modo, M. *Curr. Opin. Organ Transplantation* **2008**, *13*, 654.
(143) Pawelczyk, E.; Arbab, A. S.; Chaudhry, A.; Balakumaran, A.; Robey, P. G.; Frank, J. A. *Stem Cells* **2008**, *26*, 1366.
(144) Na, H. B.; Song, I. C.; Hyeon, T. *Adv. Mater.* **2009**, *21*, 2133.
(145) Hadjipanayis, C. J.; Bonder, M. J.; Balakrishnan, S.; Wang, X.; Mao, H.; Hadjipanayis, G. C. *Small* **2008**, *4*, 1925.
(146) Lee, J.-H.; Huh, Y.-M.; Jun, Y.-w.; Seo, J.-w.; Jang, J.-t.; Song, H.-T.; Kim, S.; Cho, E.-J.; Yoon, H.-G.; Suh, J.-S.; Cheon, J. *Nat. Med.* **2007**, *13*, 95.
(147) Jun, Y.-W.; Seo, J.-W.; Cheon, J. *Acc. Chem. Res.* **2008**, *41*, 179.
(148) Delli Castelli, D.; Terreno, E.; Cabella, C.; Chaabane, L.; Lanzardo, S.; Tei, L.; Visigalli, M.; Aime, S. NMR Biomed. 2009, http://www.dx.doi.org/10.1002/nbm.1416.
(149) Weizenecker, J.; Gleich, B.; Rahmer, J.; Dahnke, H.; Borgert, J. *Phys. Med. Biol.* **2009**, *54*, L1.
(150) Terreno, E.; Delli Castelli, D.; Aime, S. *Contrast Media Mol. Imaging*, **2010**, *5*, 78.
(151) Viswanathan, S.; Kovacs, Z.; Ratnakar, S. J.; Green, K. N.; Sherry, A. D. Chem. Rev., in press.
(152) (a) Sun, P. Z.; Murata, Y.; Lu, J.; Wang, X.; Lo, E. H.; Sorensen, A. G. *Magn. Reson. Med.* **2008**, *59*, 1175. (b) Liu, G.; Ali, M. M.; Yoo, B.; Griswold, M. A.; Tkach, J. A.; Pagel, M. D. *Magn. Reson. Med.* **2009**, *61*, 399. (c) Dixon, W. T.; Hancu, I.; Ratnakar, S. J.; Sherry, A. D.; Lenkinski, R. E.; Alsop, D. C. *Magn. Reson. Med.* **2010**, *63*, 253.
(153) Collins, C. M.; Li, S.; Smith, M. B. *Magn. Reson. Med.* **1998**, *40*, 847.
(154) Li, A. X.; Wojciechowski, F.; Suchy, M.; Jones, C. K.; Hudson, R. H. E.; Menon, R. S.; Bartha, R. *Magn. Reson. Med.* **2008**, *59*, 374.
(155) Meser Ali, M.; Yoo, B.; Pagel, M. D. *Mol. Pharm.* **2009**, *6*, 1409.
(156) Terreno, E.; Delli Castelli, D.; Cravotto, G.; Milone, L.; Aime, S. *Invest. Radiol.* **2004**, *39*, 235.
(157) Zhe Sun, P.; Farrar, C. T.; Sorensen, A. G. *Magn. Reson. Med.* **2007**, *58*, 1207.
(158) Kim, M.; Gillen, J.; Landman, B. A.; Zhou, J. Y.; van Zijl, P. C. M. *Magn. Reson. Med.* **2009**, *61*, 1441.
(159) Stancanello, J.; Terreno, E.; Delli Castelli, D.; Cabella, C.; Uggeri, F.; Aime, S. *Contrast Media Mol. Imaging* **2008**, *3*, 136.
(160) Williamson, D. C.; Narvainen, J.; Hubbard, P. L.; Kauppinen, R. A.; Morris, G. A. *J. Magn. Reson.* **2006**, *183*, 203.
(161) Vinogradov, E.; Zhang, S.; Lubag, A.; Balschi, J. A.; Sherry, A. D.; Lenkinski, R. E. *J. Magn. Reson.* **2005**, *176*, 54.
(162) Li, A. X.; Suchy, M.; Jones, C. K.; Hudson, R. H. E.; Menon, R. S.; Bartha, R. *Magn. Reson. Med.* **2009**, *62*, 1282.
(163) Vinogradov, E.; He, H.; Lubag, A.; Balschi, J. A.; Sherry, A. D.; Lenkinski, R. E. *Magn. Reson. Med.* **2007**, *58*, 650.
(164) Vinogradov, E.; Soesbe, T. C.; Balschi, J. A.; Sherry, A. D.; Lenkinski, R. E. *Proc. Int. Soc. Magn. Res. Med.* **2009**, 186.
(165) Goffeney, N.; Bulte, J. W. M.; Duyn, J.; Bryant, L. H., Jr.; van Zijl, P. C. M. *J. Am. Chem. Soc.* **2001**, *123*, 8628.
(166) Aime, S.; Delli Castelli, D.; Terreno, E. *Angew. Chem., Int. Ed.* **2003**, *42*, 4527.
(167) Snoussi, K.; Bulte, J. W. M.; Gueron, M.; van Zijl, P. C. M. *Magn. Reson. Med.* **2003**, *49*, 998.
(168) Pikkemaat, J. A.; Wegh, R. T.; Lamerichs, R.; van de Molengraaf, R. A.; Langereis, S.; Burdinski, D.; Raymond, A. Y. F.; Janssen, H. M.; de Waal, B. F. M.; Willard, N. P.; Meijer, E. W.; Gruell, H. *Contrast Media Mol. Imaging* **2007**, *2*, 229.
(169) Wu, Y.; Zhou, J.; Ouari, O.; Woods, M.; Zhao, P.; Soesbe, T. D.; Kiefer, G. E.; Sherry, A. D. *J. Am. Chem. Soc.* **2008**, *130*, 13584.
(170) Vasalatiy, O.; Gerard, R. D.; Zhao, P.; Sun, X.; Sherry, A. D. *Bioconjugate Chem.* **2008**, *19*, 598.
(171) Winter, P. M.; Cai, K.; Chen, J.; Adair, C. R.; Kiefer, G. E.; Athey, F. S.; Gaffney, P. J.; Buff, C. E.; Robertson, J. D.; Caruthers, S. D.; Wickline, S. A.; Lanza, G. M. *Magn. Reson. Med.* **2006**, *56*, 1384.
(172) Aime, S.; Delli Castelli, D.; Terreno, E. *Angew. Chem., Int. Ed.* **2005**, *44*, 5513.
(173) Zhao, J. M.; Har-el, Y.-e.; McMahon, M. T.; Zhou, J.; Sherry, A. D.; Sgouros, G.; Bulte, J. W. M.; van Zij, P. C. M. *J. Am. Chem. Soc.* **2008**, *130*, 5178.
(174) Terreno, E.; Delli Castelli, D.; Violante, E.; Sanders, H. M. H. F.; Sommerdijk, N. A. J. M.; Aime, S. *Chem.—Eur. J.* **2009**, *15*, 1440.
(175) Terreno, E.; Sanino, A.; Carrera, C.; Delli Castelli, D.; Giovenzana, G. B.; Lombardi, A.; Mazzon, R.; Milone, L.; Visigalli, M.; Aime, S. *J. Inorg. Biochem.* **2008**, *102*, 1112.
(176) Terreno, E.; Barge, A.; Beltrami, L.; Cravotto, G.; Delli Castelli, D.; Fedeli, F.; Jebasingh, B.; Aime, S. *Chem. Commun.* **2008**, 600.
(177) Chu, S. C.-K.; Xu, Y.; Balschi, J. A.; Springer, C. S., Jr. *Magn. Reson. Med.* **1990**, *13*, 239.
(178) Prosser, R. S.; Shiyanovskaya, I. V. *Concepts Magn. Reson.* **2001**, *13*, 19.
(179) Terreno, E.; Cabella, C.; Carrera, C.; Delli Castelli, D.; Mazzon, R.; Rollet, S.; Stancanello, J.; Visigalli, M.; Aime, S. *Angew. Chem., Int. Ed.* **2007**, *46*, 966.
(180) Aime, S.; Delli Castelli, D.; Terreno, E. *Methods Enzymol.* **2009**, *464*, 193.
(181) Terreno, E.; Delli Castelli, D.; Milone, L.; Rollet, S.; Stancanello, J.; Violante, E.; Aime, S. *Contrast Media Mol. Imaging* **2008**, *3*, 38.
(182) Langereis, S.; Keupp, J.; van Velthoven, J. L. J.; de Roos, I. H. C.; Burdinski, D.; Pikkemaat, J. A.; Gruell, H. *J. Am. Chem. Soc.* **2009**, *131*, 1380.
(183) Terreno, E.; Cittadino, E.; Delli Castelli, D.; Mainini, F.; Sanino, A.; Torres, E.; Aime, S. World Molecular Imaging Congress Proceedings, 2008, presentation 1522.
(184) McMahon, M. T.; Gilad, A. A.; DeLiso, M. A.; Berman, S. D. C.; Bulte, J. W. M.; van Zijl, P. C. M. *Magn. Reson. Med.* **2008**, *60*, 803.
(185) Aime, S.; Carrera, C.; Delli Castelli, D.; Geninatti Crich, S.; Terreno, E. *Angew. Chem., Int. Ed.* **2005**, *44*, 1813.
(186) Viswanathan, S.; Ratnakar, S. J.; Green, K. N.; Kovacs, Z.; De Leon-Rodriguez, L. M.; Sherry, A. D. *Angew. Chem., Int. Ed.* **2009**, *48*, 9330.
(187) Mehta, R. C.; Pike, G. B.; Enzmann, D. R. *Top. Magn. Reson. Imaging* **1996**, *8*, 214.
(188) Man-Cheuk Ng, M.-C.; Hua, J.; Hu, Y.; Luk, K. D.; Lam, E. Y. *J. Magn. Reson. Imaging* **2009**, *29*, 523.
(189) Li, A. X.; Hudson, R. H. E.; Barrett, J. W.; Jones, C. K.; Pasternak, S. H.; Bartha, R. *Magn. Reson. Med.* **2008**, *60*, 1197.
(190) Terreno, E.; Stancanello, J.; Longo, D.; Delli Castelli, D.; Milone, L.; Sanders, H. M. H. F.; Kok, M. B.; Uggeri, F.; Aime, S. *Contrast Media Mol. Imaging* **2009**, *4*, 237.
(191) Schlemmer, H. P.; Becker, M.; Bachert, P.; Dietz, A.; Rudat, V.; Vanselow, B.; Wollensack, P.; Zuna, I.; Knopp, M. V.; Weidauer, H.; Wannenmacher, M.; van Kaick, G. *Cancer Res.* **1999**, *59*, 2363.
(192) Noth, U.; Grohn, P.; Jork, A.; Zimmermann, U.; Haase, A.; Lutz, J. *Magn. Reson. Med.* **1999**, *42*, 1039.
(193) Joseph, P. M.; Fishman, J. E.; Mukherji, B.; Sloviter, H. A. *J. Comput. Assisted Tomogr.* **1985**, *9*, 1012.
(194) Higuchi, M.; Iwata, N.; Matsuba, Y.; Sato, K.; Sasamoto, K.; Saido, T. C. *Nat. Neurosci.* **2005**, *8*, 527.
(195) Waters, E. A.; Chen, J.; Allen, J. S.; Zhang, H.; Lanza, G. M.; Wickline, S. A. *J. Cardiovasc. Magn. Reson.* **2008**, *10*, 43.
(196) Srinivas, M.; Morel, P. A.; Ernst, L. A.; Laidlaw, D. H.; Ahrens, E. T. *Magn. Reson. Med.* **2007**, *58*, 725.
(197) Hunjan, S.; Zhao, D.; Canstandtinescu, A.; Hahan, E. W.; Antich, P. P.; Mason, R. P. *Int. J. Radiat. Oncol. Biol. Phys.* **2001**, *49*, 1097.
(198) Fan, X.; River, J. N.; Zamora, M.; Al-Hallaq, H. A.; Karczmar, G. S. *Int. J. Radiat. Oncol. Biol. Phys.* **2002**, *54*, 1202.
(199) Ratner, A. V.; Quay, S.; Muller, H. H.; Simpson, B. B.; Hurd, R.; Young, S. W. *Invest Radiol.* **1989**, *24*, 224.
(200) Terreno, E.; Botta, M.; Dastrù, W.; Aime, S. *Contrast Media Mol. Imaging* **2006**, *1*, 101.
(201) Neubauer, A. M.; Myerson, J.; Caruthers, S. D.; Hockett, F. D.; Winter, P. M.; Chen, J.; Gaffney, P. J.; Robertson, D.; Lanza, G. M.; Wickline, S. A. *Magn. Reson. Med.* **2008**, *60*, 1066.
(202) Kenwright, A. M.; Kuprov, I.; De Luca, E.; Parker, D.; Pandya, S. U.; Senanayake, P. K.; Smith, D. G. *Chem. Commun.* **2008**, 2514.
(203) Partlow, K. C.; Chen, J.; Brant, J. A.; Neubauer, A. M.; Meyerrose, T. E.; Creer, M. H.; Nolta, J. A.; Caruthers, S. D.; Lanza, G. M.; Wickline, S. A. *FASEB J.* **2007**, *21*, 1647.
(204) Kodibagkar, V. D.; Yu, J.; Liu, L.; Hetherington, H. P.; Mason, R. P. *Magn. Reson. Imaging* **2006**, *24*, 959.
(205) Liu, L.; Kodibagkar, V. D.; Yu, J. X.; Mason, R. P. *FASEB J.* **2007**, *21*, 2014.
(206) Capuani, S.; Porcari, P.; Fasano, F.; Campanella, R.; Maraviglia, B. *Magn. Reson. Imaging* **2008**, *26*, 987.
(207) Gadian, D. G. *NMR and its Applications to Living Systems*; Oxford University Press: Oxford, 1995.
(208) Muller, S.; Beckmann, N. *Magn. Reson. Med.* **1989**, *12*, 400.
(209) Harris, R. K. In *Nuclear Magnetic Resonance Spectroscopy*; Pitman: London, 1983.
(210) Kalechofsky, N. F. Patent No. WO 01/55656, 2001.
(211) Altes, T. A.; Salerno, M. *J. Thoracic Imaging* **2004**, *19*, 250.
(212) Oros, A. M.; Shah, N. J. *Phys. Med. Biol.* **2004**, *49*, R105.

(213) Callot, V.; Canet, E.; Brochot, J.; Viallon, M.; Humblot, H.; Briguet, A.; Tournier, H.; Cremillieux, Y. *Magn. Res. Med.* **2001**, *46*, 535.
(214) Callot, V.; Canet, E.; Brochot, J.; Berthezene, Y.; Viallon, M.; Humblot, H.; Briguet, A.; Tournier, H.; Cremillieux, Y. *Magn. Reson. Mater. Phys., Biol. Med.* **2001**, *12*, 16.
(215) Bartik, K.; Luhmer, M.; Dutasta, P.; Collet, A.; Reisse, J. *J. Am. Chem. Soc.* **1998**, *120*, 784.
(216) Schroder, L.; Lowery, T. J.; Hilty, C.; Wemmer, D. E.; Pines, A. *Science* **2006**, *314*, 446.
(217) Schlundt, A.; Kilian, W.; Beyermann, M.; Sticht, J.; Gunther, S.; Hopner, S.; Falk, K.; Roetzschke, O.; Mitschang, L.; Freund, C. *Angew. Chem., Int. Ed.* **2009**, *48*, 4142.
(218) Abragam, A.; Goldman, M. *Rep. Prog. Phys.* **1978**, *41*, 395.
(219) Comment, A.; van den Brandt, B.; Uffmann, K.; Kurdzesau, F.; Jannin, S.; Konter, J. A.; Hautle, P.; Wenckebach, W. T.; Gruetter, R.; van der Klink, J. J. *Concepts Magn. Reson., Part B* **2007**, *31B*, 255.
(220) Ardenkjaer-Larsen, J. H.; Fridlund, B.; Gram, A.; Hansson, G.; Hansson, L.; Lerche, M. H.; Servin, R.; Thaning, M.; Golman, K. *Proc. Natl. Acad. Sci. U.S.A.* **2003**, *100*, 10158.
(221) Hu, J. Z.; Solum, M. S.; Wind, R. A.; Nilsson, B. L.; Peterson, M. A.; Pugmire, R. J.; Grant, D. M. *J. Phys. Chem. A* **2000**, *104*, 4413.
(222) Hall, D. A.; Maus, D. C.; Gerfen, G. J.; Inati, S. J.; Becerra, L. R.; Dahlquist, F. W.; Griffin, R. G. *Science* **1997**, *276*, 930.
(223) Gabellieri, C.; Reynolds, S.; Lavie, A.; Payne, G. S.; Leach, M. O.; Eykyn, T. R. *J. Am. Chem. Soc.* **2008**, *130*, 4598.
(224) Merritt, M. E.; Harrison, C.; Kovacs, Z.; Kshirsagar, P.; Malloy, C. R.; Sherry, A. D. *J. Am. Chem. Soc.* **2007**, *129*, 12942.
(225) Reeder, S. B.; Brittain, J. H.; Grist, T. M.; Yen, Y.-F. *J. Magn. Reson. Imaging* **2007**, *26*, 1145.
(226) Cunningham, C. H.; Chen, A. P.; Albers, M. J.; Kurhanewicz, J.; Hurd, R. E.; Yen, Y.-F.; Pauly, J. M.; Nelson, S. J.; Vigneron, D. B. *J. Magn. Reson.* **2007**, *187*, 357.
(227) Larson, P. E. Z.; Kerr, A. B.; Chen, A. P.; Lustig, M. S.; Zierhut, M. L.; Hu, S.; Cunningham, C. H.; Pauly, J. M.; Kurhanewicz, J.; Vigneron, D. B. *J. Magn. Reson.* **2008**, *194*, 121.
(228) Chen, A. P.; Kurhanewicz, J.; Bok, R.; Xu, D.; Joun, D.; Zhang, V.; Nelson, S. J.; Hurd, R. E.; Vigneron, D. B. *Magn. Reson. Imaging* **2008**, *26*, 721.
(229) Gallagher, F. A.; Kettunen, M. I.; Day, S. E.; Lerche, M.; Brindle, K. M. *Magn. Reson. Med.* **2008**, *60*, 253.
(230) Gallagher, F. A.; Kettunen, M. I.; Day, S. E.; Hu, D.-E.; Ardenkjær-Larsen, J. H.; Zandt, R.; Jensen, P. R.; Karlsson, M.; Golman, K.; Lerche, M. H.; Brindle, K. M. *Nature* **2008**, *453*, 940.
(231) Gallagher, F. A.; Kettunen, M. I.; Hu, D.-E.; Jensen, P. R.; Zandt, R.; Karlsson, M.; Gisselsson, A.; Nelson, S. K.; Witney, T. H.; Bohndiek, S. E.; Hansson, G.; Peitersen, T.; Lerche, M. H.; Brindle, K. M. *Proc. Natl. Am. Soc.* **2009**, *106*, 19801.
(232) Jensen, P. R.; Karlsson, M.; Meier, S.; Duus, M. O.; Lerche, M. H. *Chem.—Eur. J.* **2009**, *15*, 10010.
(233) Golman, K.; Zandt, R.; Lerche, M.; Perhson, R.; Ardenkjaer-Larsen, H. *Cancer Res.* **2006**, *66*, 10855.
(234) Chen, A. P.; Albers, M. J.; Cunningham, C. H.; Kohler, S. J.; Yen, Y.-F.; Hurd, R. E.; Tropp, J.; Bok, R.; Pauly, J. M.; Nelson, S. J. *Magn. Reson. Med.* **2007**, *58*, 1099.
(235) Kohler, S. J.; Yen, Y.; Wolber, J.; Chen, A. P.; Albers, M. J.; Bok, R.; Zhang, V.; Tropp, J.; Nelson, S.; Vigneron, D. B. *Magn. Reson. Med.* **2007**, *58*, 65.
(236) Albers, M. J.; Bok, R.; Chen, A. P.; Cunningham, C. H.; Zierhut, M. L.; Zhang, V. Y.; Kohler, S. J.; Tropp, J.; Hurd, R.; Yen, Y.-F. *Cancer Res.* **2008**, *68*, 8607.
(237) Nelson, S. J.; Vigneron, D.; Kurhanewicz, J.; Chen, A.; Bok, R.; Hurd, R. *Appl. Magn. Reson.* **2008**, *34*, 533.
(238) Day, S. E.; Kettunen, M. I.; Gallagher, F. A.; Hu, D.-E.; Lerche, M.; Wolber, J.; Golman, K.; Ardenkjaer-Larsen, J. H.; Brindle, K. M. *Nat. Med.* **2007**, *13*, 1382.
(239) Witney, T. H.; Kettunen, M. I.; Day, S. E.; Hu, D.-E.; Neves, A. A.; Gallagher, F. A.; Fulton, S. M.; Brindle, K. M. *Neoplasia* **2009**, *11*, 574.
(240) Merritt, M. E.; Harrison, C.; Storey, C.; Jeffrey, F. M.; Sherry, A. D.; Malloy, C. R. *Proc. Natl. Acad. Sci. U.S.A.* **2007**, *104*, 19773.
(241) Merritt, M. E.; Harrison, C.; Storey, C.; Sherry, A. D.; Malloy, C. R. *Magn. Reson. Med.* **2008**, *60*, 1029.
(242) Schroeder, M. A.; Cochlin, L. E.; Heather, L. C.; Clarke, K.; Radda, G. K.; Tyler, D. J. *Proc. Natl. Acad. Sci. U.S.A.* **2008**, *105*, 12051.
(243) Golman, K.; Petersson, J. S.; Magnusson, P.; Johansson, E.; Åkeson, P.; Chai, C.-M.; Hansson, G.; Månsson, S. *Magn. Reson. Med.* **2008**, *59*, 1005.
(244) Schroeder, M. A.; Atherton, E. J.; Cochlin, L. E.; Clarke, K.; Radda, G. K.; Tyler, D. J. *Magn. Reson. Med.* **2009**, *61*, 1007.
(245) Schroeder, M. A.; Atherton, H. J.; Ball, D. R.; Cole, M. A.; Heather, L. C.; Griffin, J. L.; Clarke, K.; Radda, G. K.; Tyler, D. J. *FASEB J.* **2009**, *23*, 2529.
(246) Chen, A. P.; Zierhut, M. L.; Bok, R.; Yen, Y.-F.; Schroeder, M. A.; Hurd, R. E.; Nelson, S. J.; Kurhanewicz, J.; Vigneron, D. B. *Mol. Imaging Biol.* **2009**, *11*, 399.
(247) Spielman, D. M.; Mayer, D.; Yen, Y.-F.; Tropp, J.; Hurd, R. E.; Pfefferbaum, A. *Magn. Reson. Med.* **2009**, *62*, 307.
(248) Bargon, J.; Natterer, J. *Prog. Nucl. Magn. Reson. Spectrosc.* **1997**, *31*, 293.
(249) Duckett, S. B.; Sleigh, C. J. *Prog. Nucl. Magn. Reson. Spectrosc.* **1999**, *34*, 71.
(250) Bower, C. R. *Encycl. Nucl. Magn. Reson.* **2002**, *9*, 750 Sensitiviy enhancement utilizing para-hydrogen. .
(251) Blazina, D.; Duckett, S. B.; Dunne, J. P.; Godard, C. *Dalton Trans.* **2004**, 2601.
(252) Duckett, S. B.; Wood, N. J. *Coord. Chem. Rev.* **2008**, *252*, 2278.
(253) Barkemeyer, J.; Haake, M.; Bargon, J. *J. Am. Chem. Soc.* **1995**, *117*, 2927.
(254) Natterer, J.; Schedletzky, O.; Barkemeyer, J.; Bargon, J. *J. Magn. Reson.* **1998**, *133*, 92.
(255) Stephan, M.; Kohlman, O.; Niessen, H. G.; Eichhorn, A.; Bargon, J. *J. Magn. Res. Chem.* **2002**, *40*, 157.
(256) Aime, S.; Gobetto, R.; Reineri, F. *J. Chem. Phys.* **2003**, *119*, 8890.
(257) Aime, S.; Gobetto, R.; Reineri, F.; Canet, D. *J. Magn. Reson.* **2006**, *178*, 184.
(258) Johannesson, H.; Axelsson, O.; Karlsson, M. C. R. *Physique* **2004**, *5*, 315.
(259) Goldman, M.; Johannesson, H. C. R. *Physique* **2005**, *6*, 575.
(260) Adams, R. W.; Aguilar, J. A.; Atkinson, K. D.; Cowley, M. J.; Elliott, P. I. P.; Duckett, S. B.; Green, G. G. R.; Khazal, I. G.; López-Serrano, J.; Williamson, D. C. *Science* **2009**, *323*, 1708.
(261) Aime, S.; Dastrù, W.; Giovenzana, G. B.; Gobetto, R.; Reineri, F.; Santelia, D.; Viale, A. *J. Am. Chem. Soc.* **2008**, *130*, 15047.
(262) Golman, K.; Axelsson, O.; Johannesson, H.; Mansson, S.; Olofsson, C.; Peteresson, J. S. *Magn. Res. Med.* **2001**, *46*, 1.
(263) Svensson, J.; Mansson, S.; Johansson, E.; Petersson, J. S.; Olsson, L. E. *Magn. Reson. Med.* **2003**, *50*, 256.
(264) Olsson, L. E.; Chai, C.-M.; Axelsson, O.; Karlsson, M.; Golman, K.; Petersson, J. S. *Magn. Res. Med.* **2006**, *55*, 731.
(265) Ishii, M.; Emami, K.; Kadlecek, S.; Petersson, J. S.; Golman, K.; Vahdat, V.; Yu, J.; Cadman, R. V.; MacDuffie-Woodburn, J.; Stephen, M.; Lipson, D. A.; Rizi, R. R. *Magn. Res. Med.* **2007**, *57*, 459.
(266) Johansson, E.; Mansson, S.; Wirestam, R.; Svensson, J.; Petersson, J. S.; Golman, K.; Stahlberg, F. *Magn. Reson. Med.* **2004**, *51*, 464.
(267) Johansson, E.; Olsson, L. E.; Månsson, S.; Petersson, J. S.; Golman, K.; Ståhlberg, F.; Wirestam, R. *Magn. Reson. Med.* **2004**, *52*, 1043.
(268) Magnusson, P.; Johansson, E.; Månsson, S.; Petersson, J. S.; Chai, C.-M.; Hansson, G.; Axelsson, O.; Golman, K. *Magn. Reson. Med.* **2007**, *57*, 1140.
(269) van Heeswijk, R. B.; Morgenthaler, F. D.; Gruetter, R. *Magn. Reson. Imaging* **2007**, *25*, 821.
(270) Gabellieri, C.; Leach, M. O.; Eykyn, T. R. *Contrast Media Mol. Imaging* **2009**, *4*, 143.
(271) Terreno, E.; Botta, M.; Boniforte, P.; Bracco, C.; Milone, L.; Mondino, B.; Uggeri, F.; Aime, S. *Chem.—Eur. J.* **2005**, *11*, 5531.
(272) van Heeswijk, R. B.; Uffmann, K.; Comment, A.; Kurdzesau, F.; Perazzolo, C.; Cudalbu, C.; Jannin, S.; Konter, J. A.; Hautle, P.; van den Brandt, B.; Navon, G.; van der Klink, J. J.; Gruetter, R. *Magn. Reson. Med.* **2009**, *61*, 1489.
(273) Svensson, J. *Acta Radiol. Suppl.* **2003**, *44* (Suppl. 429), 1.
(274) Levin, Y. S.; Mayer, D.; Yen, Y.-F.; Hurd, R. E.; Spielman, D. M. *Magn. Reson. Med.* **2007**, *58*, 245.

CR100025T